

RESEARCH ARTICLE

# Depressional runoff cascade networks of the Des Moines Lobe of Iowa

David I. S. Green  | William G. Crumpton

Department of Ecology, Evolution, and Organismal Biology, Iowa State University, Ames, Iowa, USA

**Correspondence**

David I. S. Green, Department of Ecology, Evolution, and Organismal Biology, Iowa State University, Ames, Iowa, USA.  
 Email: [dgreen1@iastate.edu](mailto:dgreen1@iastate.edu)

## Abstract

In this study, we develop a general mathematical framework and algorithm for routing cumulative precipitation excess through depressional fill-spill cascade networks in a landscape using only information about depression morphology, local contributing areas, and potential overland flow pathways. The framework also allows for the classification of depressions according to their landscape position within a network, and calculation of precipitation- and non-precipitation-dependent network properties, including measures of network complexity and runoff connectivity. To demonstrate its use, we applied our framework to the 167,287 drained depressions of the Des Moines Lobe of Iowa, a sub-region of the Prairie Pothole Region of North America, over a large range of historically observed precipitation amounts for scenarios both neglecting and incorporating infiltration in runoff generation. Our results show that 85.3% of depressions in this region form 18,851 unique depressional runoff cascade networks, with the remainder being disjunct features. Most of the properties of the region's networks appear to conform to either a truncated power-law or lognormal distribution. For a given rainfall amount, surface runoff connectivity between depressions within networks, and between networks and off-network areas, is controlled primarily by available aggregate depressional volumetric storage and contributing area, and to a lesser degree, network complexity.

## KEY WORDS

algorithms, depressions, fill-spill cascades, network flow routing, runoff, surface water hydrology, wetlands

## 1 | INTRODUCTION

Runoff generation within and from watersheds has long been thought to occur continuously and seamlessly across spatial and temporal scales in response to precipitation events. However, results from recent field and modeling studies challenge this traditional viewpoint (see McDonnell et al., 2021; Spence, 2010 and references therein). Instead, it has been proposed that watershed runoff generation across spatial

Paper No. JAWR-21-0187-P of the *Journal of the American Water Resources Association* (JAWR).

Discussions are open until six months from publication.

This is an open access article under the terms of the [Creative Commons Attribution-NonCommercial-NoDerivs](#) License, which permits use and distribution in any medium, provided the original work is properly cited, the use is non-commercial and no modifications or adaptations are made.

© 2023 The Authors. *Journal of the American Water Resources Association* published by Wiley Periodicals LLC on behalf of American Water Resources Association.

## Research impact statement

Overland flow connectivity of depressional runoff cascade networks of the Des Moines Lobe of Iowa is controlled by aggregate depressional storage and contributing area and, to a lesser degree, network complexity.

and temporal scales occurs primarily as the result of the aggregate behavior of flow-linked “fill-spill” processes that occur between the hydrologically connected subsystems of catchments, such as soils and their unique horizons, overland flow paths, and surface depressions (McDonnell et al., 2021; Spence, 2010). In this model, outflows from a subsystem in response to one or more inflows occurs or increases substantially once a water storage threshold has been exceeded (McDonnell et al., 2021; Spence, 2010). At the watershed scale where hydrological compartments are connected, as though in a network, the aggregate behavior of these storage thresholds, defined by their hydrological connectivity and the magnitudes and durations of their respective inflows and outflows, typically manifest as nonlinear, and in some cases hysteretic relationships between precipitation, storage, and runoff (Shook & Pomeroy, 2011; Spence, 2007). Threshold-controlled flow connectivity between subsystems occurs across all catchment scales, from soil pore spaces and surface micro topographic depressions (Chu et al., 2013), to individual and networked surface and subsurface flow-connected storage basins at the macro-scale (Hayashi et al., 2016; Leibowitz & Vining, 2003; Shaw et al., 2013; Shook et al., 2021; among others). This “storage threshold” model of flow routing through complex, integrated hydrological systems has recently been recognized as having significant implications for developing a better understanding of the conditions under which catchment subsystems are hydrologically connected; an issue of considerable regulatory and public policy importance, particularly in the United States (U.S.; Alexander, 2015; Rains et al., 2016).

Depressional wetlands, such as those located throughout the Prairie Pothole Region (PPR) of North America are a prime example of threshold-controlled hydrological systems. The PPR is a unique landscape characterized by millions of permanent and ephemeral, surface and subsurface flow-connected depressions formed following the last glacial period (~11,000 years before present). These ecosystems provide critical habitat for waterfowl and other wildlife (van der Valk, 2005), act as biogeochemical hotspots (Marton et al., 2015), and are important sources of groundwater and surface water in the region (Hayashi et al., 2016; LaBaugh et al., 1998).

The hydrology of these systems varies significantly across the PPR, being primarily dependent on the balance between local or regional climate and rainfall patterns, upland and wetland plant community composition, and geology and topography (LaBaugh et al., 1998; van der Valk, 2005). These factors in turn individually and in concert determine the water balance dynamics of depressions by affecting evapotranspiration rates within wetlands and their catchments, runoff generation within surrounding uplands, exchanges with groundwater and shallow subsurface through-flow, and surface and subsurface flow connections (Hayashi et al., 2016). Likewise, wetland condition varies significantly across the region, from relatively hydrologically and ecologically intact depressional ecosystems in some areas of the north-central U.S. and Canada (van der Valk, 2005), to nearly complete degradation in others areas, such as southwestern Minnesota and north-central Iowa, resulting primarily from agricultural production (Bishop et al., 1998; Miller et al., 2012).

Depressional wetlands tend to be part of larger hydrologically connected networks, and under some conditions collectively exhibit complex nonlinear threshold-controlled overland flow cascade and shallow subsurface flow connections (Haque et al., 2018; Shaw et al., 2012, 2013; Shook et al., 2021; Shook & Pomeroy, 2011). Runoff generated within and from these depressional cascade networks is mediated by the filling and spilling of individual depressions, wherein wetland basins can export water in excess of their available storage capacities to downslope receiving systems if the difference between their inflows and outflows exceed what they can individually store, depending on antecedent water levels. The degree of filling and spilling of flow-linked depressions is in turn a function of the spatial arrangement of these features on the landscape, available depressional volumetric storage, and the amount of surface and shallow subsurface flow generated within and upslope of each depression (Haque et al., 2018; Hayashi et al., 2016; Shook et al., 2021; Stichling & Blackwell, 1957). Under high precipitation inputs, the hydrological connectivity between depressions in flow cascade networks will tend to expand, resulting in concomitant increases in runoff contributing areas and runoff from these networks. Conversely, during periods of drought, the hydrological connectedness of these systems will contract, resulting in a reduction in potential runoff contributing areas and runoff from these systems (Shaw et al., 2012; Stichling & Blackwell, 1957). This dynamic moderation of runoff dictates the timing and extent of hydrological connectivity of depressions within flow-connected networks and between networks and downstream areas, potentially affecting the magnitude and timing of surface runoff from catchments with depressional storage (Evenson et al., 2018; Grimm & Chu, 2018; Haan & Johnson, 1968; Phillips et al., 2011), as well as the transport of organisms and nutrients between depressions and from depressional networks to downslope receiving systems (Leibowitz & Vining, 2003).

Assessing the roles that depressions have in influencing rainfall-runoff processes in landscapes such as the PPR is a complex task, typically undertaken by empirical in-field observations, remote sensing analyses, or by employing semi-distributed or fully spatially distributed time-varying rainfall-runoff models. Each of these approaches provides unique scale-specific information about depressional connectivity and the processes that govern it. For example, Leibowitz et al. (2016), Haque et al. (2018), Roth and Capel (2012), Leibowitz and Vining (2003), and

Stichling and Blackwell (1957), among others have documented fill-spill behavior between depressional wetlands, providing empirical confirmation of this phenomena. Fill-spill dynamics have also been documented outside of the PPR for non-depressional wetland and subsurface flow systems (McLaughlin et al., 2019; Phillips et al., 2011; Tromp-van Meerveld & McDonnell, 2006; among others). Empirical studies of wetland connectivity in the PPR have also been expanded to larger spatial scales through remote sensing analyses alone (Vanderhoof et al., 2016), and in conjunction with in-field sampling of stable isotopes (Brooks et al., 2018), further confirming connectivity patterns observed at smaller scales. Likewise, numerous researchers have developed and implemented moderately large-scale models of fill-spill processes for catchments with depressional storage, which have yielded significant insights into how these systems dynamically affect runoff at spatial and temporal scales greater than what can be practically observed in a field setting. For instance, Evenson et al. (2018), Chu et al. (2013), Shaw et al. (2013), Huang et al. (2013), and Haan and Johnson (1968), among others, have successfully simulated depressional fill-spill cascades for various areas throughout the PPR, and each found that the cascading movement of water through these systems can have significant effects on the magnitude and timing of streamflow in the region, further confirming empirical studies of these processes.

Much of the prior work in the PPR on this topic, only some of which has been discussed here, has helped to document and predict depressional flow connectivity in this landscape, and to assess the effects this connectivity has on ecosystem functioning and regional hydrology. As valuable as this work is, much of it is constrained to detailed studies at the individual wetland or wetland complex scales, or to simulations of moderately sized catchments, such as the 1500 km<sup>2</sup> Pipestem River watershed in North Dakota studied by Evenson et al. (2018). The benefits of small- and intermediate-scale empirical monitoring and medium-scale dynamic hydrological modeling notwithstanding, there has been recognition of the need for additional, scalable, approaches to quantifying water and geochemical transfers between flow-connected systems in complex landscapes, and to develop additional metrics for characterizing these connections (Bracken & Croke, 2007; Jones et al., 2018; Leibowitz et al., 2018; McDonnell, 2013; Spence, 2010). With respect to depressional wetlands, such an approach would ideally be suitable for assessing fill-spill processes within and from, and characterizing the properties of, cascade networks in varied landscapes, ranging in scale from wetland complexes comprised of a few systems, up to the scale of the distinct sub-regions of the PPR or larger (see, e.g., Driscoll et al., 2020). While significant progress has been made toward applying a network-based approach to the analysis of hydrological connectivity between depressional wetlands and between wetlands and stream channels and other non-depressional systems (Barnes et al., 2020, 2021; Cohen et al., 2016; Shaw et al., 2013, Shook et al., 2021; Wu & Lane, 2017; among others), these approaches fail to fully account for the numerous complex pathways by which water is transported to and enters and leaves depressions.

In this work, we develop a general mathematical framework and algorithm for routing cumulative precipitation-derived surface runoff through depressional cascade networks of arbitrary size and connectivity complexity using only information about the morphological characteristics of depressions, the areas of their local catchments, their antecedent water storages, and their potential overland flow connectivity. As part of this framework, we also propose a method for classifying depressions according to their landscape positions within depressional cascade networks.

Our algorithm employs a time-integrated representation of the water balances of flow-connected depressions within a given network, and simulates the sequential routing of spatially uniform and non-uniform precipitation excess through each depression within a network. As formulated, for a given network, this framework permits the simple calculation of, as functions of precipitation, the total area of the network contributing runoff to off-network, receiving systems, the total volume of water exported by the network from depressional fill-spill controlled contributing areas, the volume of runoff stored within individual depressions in the network, and the degree of surface runoff connectivity between depressions in the network.

The proposed framework is flexible and simple enough to be used to evaluate the surface runoff properties of depressional cascade networks, for any precipitation amount, at scales ranging from a single network comprised of a few depressions, to all of the networks within a much larger region with potentially thousands to hundreds of thousands of depressions. To demonstrate its use over a range of spatial scales, we used the framework to construct the depressional cascade networks of all presently drained and morphologically intact depressions within the Des Moines Lobe of Iowa (DML-IA), a sub-region of the PPR contained within the state of Iowa, USA. The framework was also used to route precipitation excess through these networks for a range of rainfall depths historically encountered in the region, for scenarios both neglecting and incorporating infiltration abstractions. In addition to presenting results of the region-wide application of our framework to the DML-IA, we also show how properties of the depressional cascade networks in this sub-region of the PPR are statistically distributed, and how network structural properties, particularly measures of complexity, influence depressional and network runoff connectivity.

## 2 | FRAMEWORK THEORY

Neglecting the effects of landscape heterogeneities on runoff generation, the movement of precipitation excess through a depressional cascade network is controlled by the spatial distributions of maximum depressional storage volumes, the sizes of local catchments, and potential surface and subsurface runoff connectivity between depressions (Shook et al., 2021). In general, depressions within a cascade network (and a cascade network with downslope off-network receiving systems) are hydrologically connected through the sequential filling and spilling

of runoff through the network, which is in turn, controlled by the water balances of individual depressions. As also described by Leibowitz et al. (2016) and others, in this conceptual framework, a given depression will fill or overspill an amount of water equal to the difference in volumes between what it receives from its local catchment from overland flow and/or exfiltration of shallow subsurface water, direct precipitation, and adjoining, directly upslope flow contributing neighboring depressions (herein referred to as “directly neighboring upslope depressions”), and what it loses to infiltration and evapotranspiration. In the case of overspill, excess runoff will be exported either to the next depression or set of depressions in the flow cascade sequence (herein referred to as “directly neighboring downslope depressions”), or, if the depression is a terminal feature representing the outlet of the network or a non-networked depression, to off-network areas. Conversely, if the difference in volumes between what the depression receives from external inputs and loses to internal outputs does not exceed available storage, the depression will be disconnected with respect to surface runoff from downslope depressions or receiving systems. When evaluated over an entire network, the sequential filling and spilling of depressions gives rise to a nonlinear dependence between precipitation inputs and network runoff contributing area, volumetric exports, and runoff connectivity (Shaw et al., 2013; Shook et al., 2021).

## 2.1 | Depressional cascade runoff routing algorithm

Consider a natural topographic depression  $i$  within a network of  $n$  depressions with storage volume and inundation area when full,  $V_{\max(i)}$  and  $A_{\max(i)}$ , and local contributing area  $A_{\text{cat}(i)}$  that receives runoff from its local catchment and some or all directly neighboring upslope flow-contributing depressions, as illustrated in Figure 1. Assuming uniform precipitation of variable intensity  $I_i(t)$  over  $i$  and its local catchment, the change in water storage volume of  $i$  as a function of time resulting from runoff generated by a single storm event can be written as:

$$\frac{dV_i}{dt} = A_{\text{cat}(i)} p_{\text{exc}(i)}(I_i(t)) + A_{\max(i)} I_i(t) + \sum_{j \in m(i)} \left( \frac{q_{\text{out}(j)}(t) - q_{\text{inf}(j,i)}(t) - q_{\text{et}(j,i)}(t)}{|k_j|} \right) + q_{\text{exf}(i)}(t) - q_{\text{out}(i)}(t) - q_{\text{inf}(i)}(t) - q_{\text{et}(i)}(t), \quad (1)$$

where  $A_{\text{cat}(i)} p_{\text{exc}(i)}(I_i(t))$  is the volumetric rate of precipitation excess generated within the local catchment of  $i$  as a function of  $I_i(t)$  and rainfall abstractions in the catchment of  $i$ ,  $q_{\text{exf}(i)}(t)$  is the rate of exfiltration of shallow groundwater into  $i$ ,  $q_{\text{out}(i)}(t)$  is the time-varying rate of surface outflow from  $i$  to downslope systems, and  $q_{\text{inf}(i)}(t)$  and  $q_{\text{et}(i)}(t)$  represent rates of infiltration and evapotranspiration from  $i$ . The term  $\sum_{j \in m(i)} \left( \frac{q_{\text{out}(j)}(t) - q_{\text{inf}(j,i)}(t) - q_{\text{et}(j,i)}(t)}{|k_j|} \right)$  represents the combined rates of overflow contributions of the set  $m$  of directly neighboring upslope depressions, accounting for the number of receiving depressions  $|k_j|$  in the set  $k$  for each directly neighboring downslope depression belonging to each upslope depression  $j$ . This term incorporates the potential loss of water exported from  $j$  to evapotranspiration ( $q_{\text{et}(j,i)}(t)$ ) and infiltration ( $q_{\text{inf}(j,i)}(t)$ ) while in transit to  $i$ .

For a single precipitation event, integrating Equation (1) from the onset of precipitation at  $t = 0$  to time  $\tau$  yields:

$$\begin{aligned} \int_0^\tau dV_i &= A_{\text{cat}(i)} \int_0^\tau p_{\text{exc}(i)}(I_i(t)) dt + A_{\max(i)} \int_0^\tau I_i(t) dt + \int_0^\tau \sum_{j \in m(i)} \left( \frac{Q_{\text{out}(j)}(t) - Q_{\text{inf}(j,i)}(t) - Q_{\text{et}(j,i)}(t)}{|k_j|} \right) dt + \int_0^\tau Q_{\text{exf}(i)}(t) dt - \int_0^\tau Q_{\text{out}(i)}(t) dt \\ &\quad - \int_0^\tau Q_{\text{inf}(i)}(t) dt - \int_0^\tau Q_{\text{et}(i)}(t) dt \rightarrow V_{\tau(i)} - V_{0(i)} = Q_{\text{cat}(i)} + Q_{\text{prc}(i)} + \sum_{j \in m(i)} \left( \frac{Q_{\text{out}(j)}(t) - Q_{\text{inf}(j,i)}(t) - Q_{\text{et}(j,i)}(t)}{|k_j|} \right) + Q_{\text{exf}(i)} - Q_{\text{out}(i)} - Q_{\text{inf}(i)} - Q_{\text{et}(i)} \end{aligned} \quad (2)$$

where  $V_{0(i)}$  is the initial volume of water stored in  $i$  ( $0 \leq V_{0(i)} \leq V_{\max(i)}$ ),  $V_{\tau(i)}$  is the volume of water stored in  $i$  at the end of the interval, and  $Q_{\text{prc}(i)}$ ,  $Q_{\text{cat}(i)}$ ,  $Q_{\text{out}(i)}$ ,  $Q_{\text{exf}(i)}$ ,  $Q_{\text{inf}(i)}$ , and  $Q_{\text{et}(i)}$  are the volume of precipitation onto  $i$ , the volume of rainfall-derived surface runoff transported to  $i$  from its local catchment, the volume of surface runoff exported from  $i$ , the volume of exfiltrated groundwater to  $i$ , the volume of water infiltrated from  $i$ , and the volume of water lost through evapotranspiration within  $i$  over the interval of integration, respectively.

The term  $V_{\tau(i)} - V_{0(i)}$  in Equation (2) represents the change in water storage of  $i$  over the integration interval. Precipitation excess for a given amount of rainfall represents the depth of precipitation remaining for potential overland flow after losses to infiltration, evapotranspiration, and interception have been taken into account. This quantity is primarily a function of the hydraulic characteristics of local soils and their antecedent moisture conditions (AMC) and local land-use patterns, and is often a nonlinear function of precipitation intensity and amount as well as storm duration. Figure 2 provides a cross-sectional view of the integrated water balances of overland flow-linked depressions and their corresponding local catchments within a general depressional cascade network.

Rearranging Equation (2) for  $Q_{\text{out}(i)}$  gives:

$$Q_{\text{out}(i)} = Q_{\text{cat}(i)} + Q_{\text{prc}(i)} + \sum_{j \in m(i)} \left( \frac{Q_{\text{out}(j)} - Q_{\text{inf}(j,i)} - Q_{\text{et}(j,i)}}{|k_j|} \right) + Q_{\text{exf}(i)} - Q_{\text{inf}(i)} - Q_{\text{et}(i)} - (V_{\tau(i)} - V_{0(i)}). \quad (3)$$

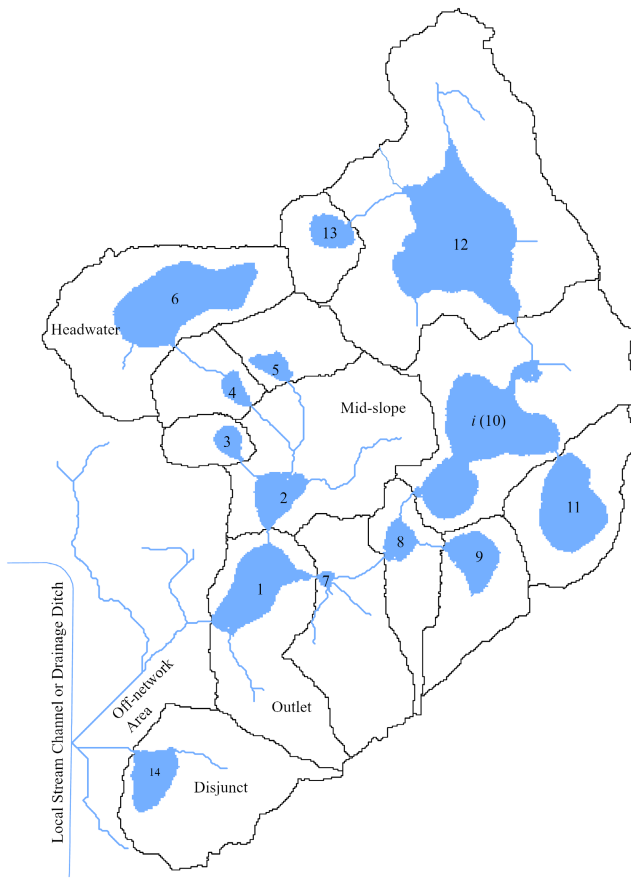


**FIGURE 1** Example of a depressional cascade network, and of a disjunct depression. The black outlined polygons represent the individual local catchments of each depression, which are represented as blue polygons. Overland flow paths are represented as blue lines. The general water balance for depression  $i$  (Equation 5), applicable to any depression in the network, is shown in Figure 2. For this network 1 is the outlet depression, 3, 5, 6, 9, 11, and 13 are headwater depressions, and 2, 4, 7, 8,  $i$  (10), and 12 are mid-slope depressions. For illustration purposes, the headwater depression 6 has directly neighboring  $|m| = 0$  upslope depressions and  $|k| = 1$  downslope depressions. Likewise, the mid-slope depressions 2 and  $i$  (10) have directly neighboring  $|m| = 3$  upslope and  $|k| = 1$  downslope depressions, and  $|m| = 2$  upslope and  $|k| = 1$  downslope depressions, respectively. This network possesses a Strahler order ( $O_{st}$ ) of 3, a Shreve order ( $O_{sh}$ ) of 6, a branching order  $O_b$  of 4, and a fractional branching order,  $f_b$ , of 0.31. The morphological characteristics, sets of directly neighboring upslope ( $m$ ) and downslope ( $k$ ) depressions for this network, and measures of network complexity for this system are given in Table 1.

Since surface outflow from  $i$  only occurs when the difference between inputs and outputs of water ( $V_{r(i)} - V_{0(i)}$ ) meets or exceeds its storage deficit ( $V_{\max(i)} - V_{0(i)}$ ), Equation (3) can be written as:

$$Q_{out(i)} = \begin{cases} 0; Q_{cat(i)} + Q_{prc(i)} + \sum_{j \in m} \left( \frac{Q_{out(j)} - Q_{inf(j,i)} - Q_{et(j,i)}}{|k_j|} \right) + Q_{exf(i)} - Q_{inf(i)} - Q_{et(i)} - (V_{\max(i)} - V_{0(i)}) \leq 0 \\ Q_{cat(i)} + Q_{prc(i)} + \sum_{j \in m} \left( \frac{Q_{out(j)} - Q_{inf(j,i)} - Q_{et(j,i)}}{|k_j|} \right) + Q_{exf(i)} - Q_{inf(i)} - Q_{et(i)} - (V_{\max(i)} - V_{0(i)}), \end{cases} \quad (4)$$

which can be expressed more compactly as:

$$Q_{out(i)} = \max \left( Q_{cat(i)} + Q_{prc(i)} + \sum_{j \in m} \left( \frac{Q_{out(j)} - Q_{inf(j,i)} - Q_{et(j,i)}}{|k_j|} \right) + Q_{exf(i)} - Q_{inf(i)} - Q_{et(i)} - (V_{\max(i)} - V_{0(i)}), 0 \right). \quad (5)$$

Equation (5) represents the basic algorithm for routing surface runoff through a depressional fill-spill cascade network resulting from surface runoff as a function of a total depth of precipitation  $P$  (equal to  $\int_0^T l(t)dt$ ), given information about depressional morphology, local depressional contributing areas, antecedent water storage within depressions, and surface flow linkages between depressions within the network. For a given network Equation (5) is solved recursively, depression-by-depression, to accumulate and route precipitation excess beginning with

the farthest downslope depression (the outlet depression) and working upslope through the remainder of the network. As such, the solution to [Equation \(5\)](#) is unique for a given depth of precipitation for each depression and its contributing area within a network, and for the total network.

## 2.2 | Depressional network structure

Depressions within a cascade network of  $n$  features can be classified as being one of four landscape position types: headwater, mid-slope, outlet, or disjunct ([Figure 1](#) and [Table 1](#)). Headwater depressions are positioned farthest upslope in the network and are defined as having  $|m| = 0$  directly neighboring upslope flow-contributing depressions, and  $|k| > 0$  directly neighboring downslope flow-receiving depressions ( $|m|$  and  $|k|$  represent the number of depressions in the sets  $m$  and  $k$  associated with each depression in the network). Mid-slope depressions exist within the middle of the network, and are defined as having  $|m| > 0$  upslope and  $|k| > 0$  downslope directly neighboring depressions. Outlet depressions are the farthest downslope features within the network, and are defined as having  $|m| > 0$  and  $|k| = 0$  directly neighboring upslope and downslope depressions. Disjunct depressions are single ( $n = 1$ ) features that are removed from larger ( $n > 1$ ) networks, and are defined as having  $|m| = 0$  and  $|k| = 0$  directly neighboring upslope and downslope depressions. For most landscapes, outlet and disjunct depressions will likely discharge to non-depressional areas that are downslope of the network, including local swales or other overland flow pathways, and local streams.

Taken together, the flow-connected arrangement of depressions on the landscape according to this conceptual framework formally constitutes a directed acyclic graph with depressions acting as nodes in the network and the overland flow connections between them as edges ([Shook et al., 2021](#)). Our proposed framework can be used as a conceptual model for considering depressional cascade networks in a manner that permits analysis of how runoff connectivity between depressions, overland flow contributing areas of depression-dominated catchments, volumetric storage within depressions, and volumetric exports from catchments characterized by threshold-controlled depressional fill-spill processes may vary with precipitation.

## 2.3 | Properties of the depressional network

Recursive application of [Equation \(5\)](#) to each of the depressions in a cascade network of size  $n$  for a given rainfall amount  $P$  yields several precipitation-dependent network properties, the most important of which is the set of depressions,  $D_{ro}$ , within the network that contribute runoff to areas downslope of the network outlet. Building from this set, we define the following:

$$n_{ro} = |D_{ro}|, f_{ro} = \frac{n_{ro}}{n}, \quad (6)$$

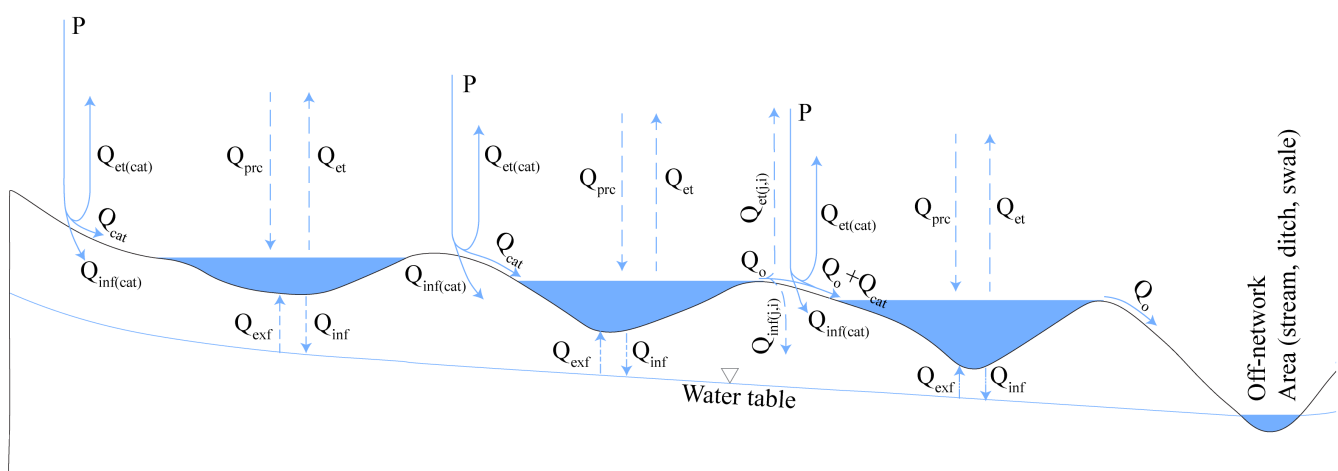


**FIGURE 2** Cross-sectional view of a generic depressional cascade network and associated integrated water balances ([Equation 2](#)).  $P$  is precipitation.  $Q_{pre}$  is direct precipitation onto depressions.  $Q_{exf}$  is exfiltration of groundwater into depressions.  $Q_{inf}$  is infiltration of water from depressions into the subsurface.  $Q_{inf(j,i)}$  and  $Q_{et(j,i)}$  are losses of water to infiltration and evapotranspiration while in transit between depressions, respectively. The quantities  $Q_{et(cat)}$  and  $Q_{inf(cat)}$  represent catchment precipitation abstractions (losses of rainfall), the remainder of which is precipitation excess ( $Q_{cat}$ ).  $Q_o$  is surface outflow from depressions. Features are not to scale: depressions have been exaggerated and catchments under sized for the purpose of illustration.

$$A_{ro} = \sum_{i \in D_{ro}} (A_{cat(i)} + A_{max(i)}), \quad f_{A_{ro}} = \frac{A_{ro}}{\sum_{i \in n} (A_{cat(i)} + A_{max(i)})} = \frac{A_{ro}}{A_{nw}}, \quad (7)$$

$$Q_{ro} = \sum_{i \in D_{ro}} (Q_{out(i)} [\text{type}_i = \text{outlet}]), \quad f_{Q_{ro}} = \frac{Q_{ro}}{Q_{tot}}, \quad (8)$$

$$V_{sto} = \sum_{i \in n} \left\{ Q_{cat(i)} + Q_{prc(i)} + \sum_{j \in m} \left( \frac{Q_{out(j)} - Q_{inf(j,i)} - Q_{et(j,i)}}{|k_j|} \right) + Q_{exf(i)} - Q_{inf(i)} - Q_{et(i)} + V_{0(i)} \right\}, \quad (9)$$

where  $n_{ro}$  and  $f_{ro}$  are the number of runoff-contributing depressions, and this quantity normalized by the size of the network, respectively.  $A_{ro}$  and  $f_{A_{ro}}$  are the cumulative network runoff contributing area, and this quantity normalized by the total network contributing area  $A_{nw}$ , respectively.  $Q_{ro}$  is the total volume of surface runoff from the network exported through the outlet depressions, and  $f_{Q_{ro}}$  is this quantity expressed as a fraction of the total volume of precipitation excess for a given precipitation amount,  $Q_{tot}$ , that would be exported from the total network contributing area absent depressional retention, and accounting for infiltration and evapotranspiration losses.  $V_{sto}$  ( $\geq 0$  and  $\leq \sum_{i \in n} V_{max(i)}$ ) is the volume of water stored in all depressions in the network as a function of  $P$ . The quantity  $f_{ro}$  is a primary metric of depressional runoff connectivity both within the network and from the network to downslope areas, and is analogous to the runoff connectivity metric proposed by Phillips et al. (2011).

We also define the following additional network properties:

$$n_{fill} = \left| \left\{ i \in n : V_{sto(i)} = V_{max(i)} \right\} \right|, \quad f_{fill} = \frac{n_{fill}}{n}, \quad (10)$$

$$f_{sto} = \frac{V_{sto}}{\sum_{i \in n} V_{max(i)}} = \frac{V_{sto}}{V_{nw}}, \quad f_{sq} = \frac{V_{sto}}{Q_{tot}}, \quad (11)$$

$$S_d = \frac{\sum_{i \in n} (V_{max(i)} - V_{0(i)})}{\sum_{i \in n} (A_{cat(i)} + A_{max(i)})} = \frac{\sum_{i \in n} (V_{max(i)} - V_{0(i)})}{A_{nw}}, \quad R_d = \frac{S_d}{P}, \quad (12)$$

where  $n_{fill}$  and  $f_{fill}$  are the number of depressions in the network that have been filled to capacity and this quantity expressed as a fraction of the network size, and  $f_{sto}$  and  $f_{sq}$  are  $V_{sto}$  expressed as a fraction of the total network depressional storage volume, and as a fraction of the volume of runoff in the absence of depressional storage, respectively.  $S_d$  and  $R_d$  in Equation (12) represent the network catchment depressional specific storage, and runoff index (Green et al., 2019). As discussed by these authors,  $S_d$  represents the depth of precipitation that is required to meet aggregate available depressional storage in the network, and  $R_d$  is a precipitation-dependent dimensionless index denoting whether that storage has been met for a given precipitation amount. If  $R_d > 1$  then excess depressional storage exists within the network. Conversely, if  $R_d \leq 1$  all depressional storage has been filled or exceeded. These two quantities account for the aggregate effect of depressional storage on surface runoff attenuation in a manner that neglects network connectivity.

These precipitation-dependent properties give information about the degree of surface runoff connectivity between depressions in the network, their runoff storage, and surface water exports for a given amount of precipitation applied over a network. In general:

$$\lim_{P \rightarrow \infty} [n_{ro}, n_{fill}] = n, \quad \lim_{P \rightarrow \infty} A_{ro} = A_{nw}, \quad \lim_{P \rightarrow \infty} V_{sto} = V_{nw}, \quad \lim_{P \rightarrow \infty} Q_{ro} = Q_{tot}, \quad (13)$$

and,

$$\lim_{P \rightarrow \infty} [f_{ro}, f_{fill}, f_{A_{ro}}, f_{sto}] = 1, \quad \lim_{P \rightarrow \infty} [f_{sq}, R_d] = 0, \quad \lim_{P \rightarrow \infty} f_{Q_{ro}} = 1, \quad (14)$$

indicating increasing degrees of hydrological connectedness between depressions in, and increasing downslope runoff contributions from, the network. Conversely:

$$\lim_{P \rightarrow 0} [n_{ro}, n_{fill}, A_{ro}, Q_{ro}] = 0, \quad \lim_{P \rightarrow 0} V_{sto} = \sum_{i \in n} (V_{0(i)} + Q_{exf(i)} - Q_{inf(i)} - Q_{ET(i)}), \quad (15)$$

and

$$\lim_{P \rightarrow 0} [f_{ro}, f_{A_{ro}}, f_{sto}] = 0, \quad \lim_{P \rightarrow 0} [f_{Q_{ro}}] = 0, \quad \lim_{P \rightarrow 0} [f_{sq}] = 1, \quad \lim_{P \rightarrow 0} [R_d] = \infty, \quad (16)$$

indicating decreasing degrees of surface runoff connectivity between depressions in the network, and runoff contributions from the network to downslope regions. Since the surface runoff connectivity of a given network results from sequential fill-spill cascades between depressions, the relationships between precipitation and these quantities within the established limits are generally nonlinear, the degree of which is a function of network structure and antecedent water storage. Network structure is in turn a function of the spatial distributions of depressions within the network and their morphological characteristics and catchment areas, as well as the complexity of their connections. The proposed network properties and their corresponding limits are also applicable to each depression within a network, as each represents the outlet of a sub-network comprised of all upslope, and potentially contributing, depressions. Conversely, these properties are also additive between networks, as this framework defines networks as distinct structures comprised of unique sets of depressions. Thus, as will be demonstrated, the framework can be applied across spatial scales to give aggregate network properties, precipitation dependent and otherwise, of all the distinct networks within a larger region. It should be noted that although  $f_{sq}$  approaches one as  $P$  approaches zero,  $f_{sq}$  is not defined at  $P = 0$  when  $V_{sto} = 0$ , and is infinity when  $V_{sto} \geq 0$ . Likewise, although  $f_{Q_{ro}}$  approaches zero when  $P$  approaches zero, this quantity is also not defined at  $P = 0$  as both  $Q_{ro}$  and  $Q_{tot}$  are also zero at the limit. However, for most practical applications, the limits listed in [Equation \(16\)](#) for these two properties hold.

## 2.4 | Measures of network complexity and structure

Because depressional cascade networks are directed acyclic graphs, their flow connectivity complexity can be defined using tree branching numbering systems, such as those devised by Strahler ([1952, 1957](#)) and Shreve ([1966](#)) for the classification of stream networks. For this work, the Strahler and Shreve network ordering algorithms were modified to account for differences between stream and depressional cascade networks, namely in their treatment of headwater features and the existence of singular connections between depressions. Building from Lanfear ([1990](#)), the general algorithm employed in this work for assigning the Strahler order ( $O_{st}$ ) to a depression  $i$  in a cascade network is written as:

$$O_{st(i)} = \begin{cases} 1; |m_i| = 0 \\ O_{st(j)}; |m_i| = 1 \\ \max_{j \in m} \{O_{st(j)}\}; |m_i| > 1 \\ O_{st(j)} + 1; \{j \in m; O_{st(j)} = O_{st}\} \wedge |m_i| > 1 \end{cases}, \quad (17)$$

where  $O_{st(i)}$  is the Strahler order of depression  $i$ ,  $m_i$  is the set of upslope directly neighboring depressions of  $i$ , and  $O_{st(j)}$  is the order of each depression in  $m_i$ . Likewise, the algorithm employed for assigning the Shreve ([1966](#)) order ( $O_{sh}$ ) to a depression  $i$  is written as:

$$O_{sh(i)} = \begin{cases} 1; |m_i| = 0 \\ O_{sh(j)}; |m_i| = 1 \\ \sum_{j \in m} O_{sh(j)}; |m_i| > 1 \end{cases}, \quad (18)$$

where  $O_{sh(i)}$  and  $O_{sh(j)}$  are the Shreve orders of  $i$  and of each directly neighboring upslope depression  $j$  of  $i$ , respectively.

For both modified ordering schemes, headwater depressions ( $|m| = 0$ ) are assigned an order of one. In the modified Strahler ordering algorithm, if a depression is connected to two or more directly neighboring upslope depressions of the same order  $O_{st}$ , as denoted by the expression  $\{j \in m; O_{st(j)} = O_{st}\} \wedge |m_i| > 1$  in [Equation \(17\)](#), then the depression is assigned an order of one plus the order of the upslope features, otherwise the depression is assigned the maximum order of all directly neighboring upslope flow-connected features. In this same case for the modified Shreve algorithm, the order of a depression is determined as the sum of the orders of each of its directly neighboring upslope depressions if the number of these features is greater than one. In both modified algorithms, a depression with a single directly neighboring upslope depression will inherit its order from that feature. In this case, each depression in a linear chain of features will possess the order of the first upslope depression in the set, whether being a headwater feature or the first depression immediately downslope of a depression with two or more contributing upslope depressions. Thus, networks that form a linear chain in which no depression is connected to more than one directly neighboring upslope and/or downslope feature will have a total network order of one for both ordering schemes.

Both the Strahler and Shreve orders of a network give an indication of the degree of branching within the system, and therefore the spatial complexity of potential flow connectivity between depressions. Another closely related measure of complexity considered in this work is the number of depressions in a network that are connected to two or more directly neighboring upslope flow-connected depressions of which each connection represents a farther upslope branch of the network (for instance, depressions 1, 2, 8, and  $i$  (10) in [Figure 1](#)). This quantity,

**TABLE 1** Table of characteristics for all depressions in the network featured in Figure 1 including maximum storage volume ( $V_{\max}$ ), maximum inundation area ( $A_{\max}$ ), maximum depth ( $H_{\max}$ ), and local catchment area ( $A_{\text{cat}}$ ). Also included is a listing of the sets of directly neighboring upslope ( $m$ ) and downslope ( $k$ ) depressions, as well as calculated Strahler order ( $O_{\text{st}}$ ; Equation 17) and Shreve order ( $O_{\text{sh}}$ ; Equation 18) for each depression. {} denotes an empty set. This table is intended to illustrate how information about depressions and their neighboring flow-connected features was used to construct cascade networks for the Des Moines Lobe Region of Iowa (DML-IA) and to route precipitation excess through these networks.  $H_{\max}$  is not used in the framework directly, but is an important attribute of these systems, and is included in this example table to provide a complete set of information about the morphology of these depressions.

Depression	Type	$V_{\max}$ (m <sup>3</sup> )	$A_{\max}$ (m <sup>2</sup> )	$H_{\max}$ (m)	$A_{\text{cat}}$ (m <sup>2</sup> )	$m$	$k$	$O_{\text{st}}$	$O_{\text{sh}}$
1	Outlet	4552.3	15,219	0.6	72,954	{2,7}	{}	3	6
2	Mid-slope	1161.1	7065	0.35	90,549	{3,4,5}	{1}	2	3
3	Headwater	531.6	2547	0.44	14,013	{}	{2}	1	1
4	Mid-slope	200.0	2322	0.29	25,317	{6}	{2}	1	1
5	Headwater	311.8	2727	0.27	29,133	{}	{2}	1	1
6	Headwater	10,424.1	26,154	0.94	89,091	{}	{4}	1	1
7	Mid-slope	40.8	774	0.20	65,133	{8}	{1}	2	3
8	Mid-slope	403.3	3699	0.31	31,248	{9,10}	{7}	2	3
9	Headwater	1712.1	7641	0.74	39,996	{}	{8}	1	1
i (10)	Mid-slope	12,364.7	35,658	0.73	122,076	{11,12}	{8}	2	2
11	Headwater	5238	16,713	0.57	50,913	{}	{10}	1	1
12	Mid-slope	21,163.8	45,963	1.08	197,109	{13}	{10}	1	1
13	Headwater	934.5	4329	0.59	22,005	{}	{12}	1	1
14	Disjunct	1103.8	7848	0.41	73,467	{}	{}	1	1

termed herein as the network branching order  $O_b$ , can be normalized by the number of depressions in the network to give a fractional branching order,  $f_b$ . As will be shown in a later section,  $O_b$  is a close approximation of the Shreve order of a network, and can be reasonably estimated by the number of depressions in a network. A network with no branching depressions will feature  $O_b$  and  $f_b$  values of zero, corresponding to  $O_{\text{st}}$  and  $O_{\text{sh}}$  values of one. In this work, and like stream systems, because flow is directional from upslope depressions to downslope depressions in depressional cascade networks, branching nodes represent points of convergence of flows from sub-networks within a larger network. As also described by Lanfear (1990), these numbering schemes can be applied to a given network recursively or iteratively, starting from the outlet depression.

For this work, the presented algorithms (Equations 5 through 18) were implemented in the Python 2.7 programming language using an object-oriented approach. However, it should be noted that these algorithms could also be easily implemented in a spreadsheet.

## 2.5 | Example application of the framework to a single cascade network

Figure 3 shows each of the defined precipitation-dependent network properties for an example 2581 ha network of 224 depressions within the DML-IA (Figure 4;  $O_{\text{st}}$  of 3,  $O_{\text{sh}}$  of 167,  $O_b$  of 46, and  $f_b$  of 0.205) for rainfall amounts between 1 and 500 mm at 10 mm increments, assuming an impervious surface throughout the network and that each depression was initially empty ( $V_0 = 0$ ). As observed for this system, the threshold-controlled sequential filling and spilling of depressions tends to result in an oft seen (e.g., Grimm & Chu, 2018; Shaw et al., 2013; Shook et al., 2021) stair-step pattern for variable contributing area and network connectivity (inferred from the fraction of depressions contributing runoff from the network  $f_{ro}$ ), reflecting the roles of depressions as runoff mediators, or threshold control points, within the network. This is particularly the case if the network features a few large depressions that only spill under high precipitation amounts, and essentially act as “gatekeepers” of runoff from large portions of the network (Shook et al., 2021).

This gatekeeping behavior can be observed in Figure 3 at the points of sudden increase in both the fraction of depressions contributing runoff to and through the outlet feature (and thus to off-network areas) and the network contributing area. In this example, numerous large gatekeeping depressions exist at the mid-slope position within the network (Figure 4), resulting in surface runoff, and therefore flow connectivity, discontinuities between regions downslope and upslope of these features until a threshold rainfall amount occurs, at which point previously disconnected areas of the network contribute flows to and through the outlet depression (Shaw et al., 2013; Shook et al., 2021).

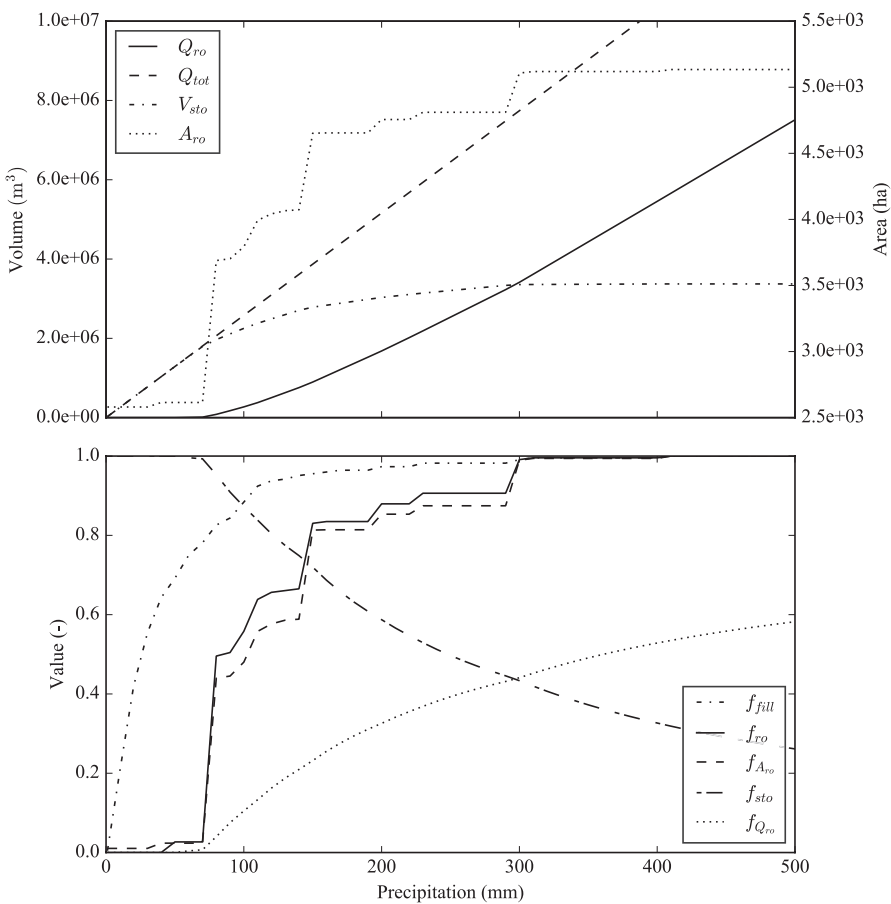


**FIGURE 3** Precipitation-dependent network properties for the example network. Top panel: volume of runoff from the network  $Q_{ro}$  ( $\text{m}^3$ ); total volume of runoff over the network,  $Q_{\text{tot}}$  ( $\text{m}^3$ ; equal to the product of  $P$  and  $A_{\text{nw}}$  in this case); the volume of runoff stored in depressions in the network,  $V_{\text{sto}}$  ( $\text{m}^3$ ), and the area of the network that is actively contributing runoff  $A_{\text{ro}}$  (ha). Bottom panel (all variables are dimensionless):  $f_{\text{fill}}$  is the fraction of depressions in the network that are filled to capacity;  $f_{\text{ro}}$  is the fraction of depressions in the network that are contributing runoff to off-network areas;  $f_{A_{\text{ro}}}$  is the fraction of the network contributing area involved in runoff generation to off-network areas;  $f_{\text{sto}}$  is the fraction of runoff stored in depressions; and  $f_{Q_{\text{ro}}}$  is the fraction of total runoff from the network.

### 3 | FRAMEWORK APPLICATION

#### 3.1 | Study area

The 31,032 km<sup>2</sup> DML-IA is the sub-region of the larger Des Moines Lobe (DML) region of the PPR that is contained within the boundaries of the state of Iowa. The DML-IA is characterized by very low relief depression-rich uplands situated between the numerous relatively narrow and deep river valleys that traverse the region from the northwest to the southeast (Figure 5). The geology of the DML-IA is marked by distinct geomorphic sub-regions, the boundaries of which are distinguished by east–west oriented bands of morainal deposits, representing the stages of glacial retreat toward the end of the last glaciation (Prior, 1991).

Soils in the region are comprised primarily of poorly and relatively poorly drained hydric types in depressions and adjacent areas, moderately well-drained sandier soils in mid and downslope areas closer to established swales and first-order stream channels, and sandy alluvial soils in floodplains (Miller et al., 2009). Much of the upland areas of the DML-IA are underlain by relatively shallow un-oxidized glacial till with low permeability (Prior, 1991).

Currently, approximately 80% of the DML-IA is underlain by extensive networks of subsurface tile drains and is in intensive row crop agricultural production, with most farming concentrated in the uplands (Green et al., 2019). Large-scale drainage has resulted in a near complete loss of depressional wetland ecological and hydrological functions in this landscape (Bishop et al., 1998; Miller et al., 2012), and most depressions in the region are perennially dry (McDeid et al., 2018; Schilling et al., 2019). However, most of these systems remain largely morphologically intact and presently possess the capacity to only intermittently store surface runoff, although not enough to have a significant effect on the magnitude of the relatively infrequent and large-scale flood events that periodically occur in the region (Neri et al., 2019).

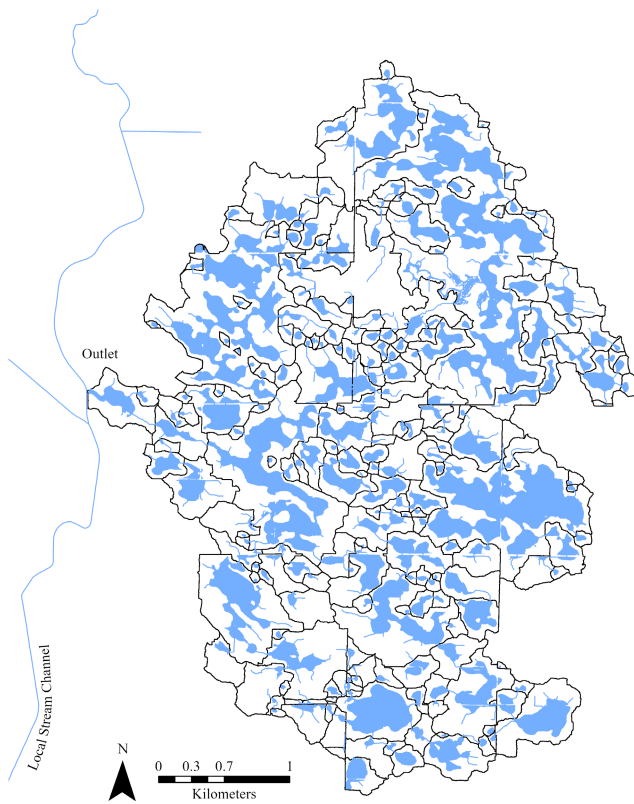


**FIGURE 4** A 2581ha network of 224 depressions given in the example application of the proposed algorithms. This network features a branching order ( $O_b$ ) of 46, comprising 20.5% of depressions in the network ( $f_b = 0.205$ ), a Strahler order ( $O_{st}$ ) of 3, and a Shreve order ( $O_{sh}$ ) of 167. The black outlined polygons represent the individual local catchments of each depression, which are represented as blue polygons. The location of this network within the DML-IA is shown in [Figure 5](#).

Tile drains alone increase infiltration and reduce surface runoff (Haan & Johnson, 1968; Schilling et al., 2019), thereby reducing the likelihood and duration that a depression will hold standing water. In addition to being underlain by subsurface tile drains, some depressions in the region also have direct surface connections through vertical intake pipes which effectively increase the rate of vertical movement of water out of the system and into underlying tile (Martin et al., 2019; Roth & Capel, 2012). For depressions with tile drainage alone, ponded water can persist for a period ranging from days to weeks. In contrast, depressions that possess vertical intake pipes can hold water typically for a period of less than a week (Roth & Capel, 2012).

The majority of rainfall in the DML-IA tends to occur during the spring months, when multi-day successive rain events are a common occurrence. Rainfall during the remainder of the year tends to occur from periodic and short-lived high-intensity storms during the summer months, some of which are intense enough to produce local flash flooding, with a transition to more frequent multi-day storms in early to mid-autumn months. Long-term average annual rainfall ranges from approximately 730mm in the northwest of the region, to nearly 910mm in the southeast (Perica et al., 2013).

### 3.2 | Morphology of depressions in the DML-IA

McDeid et al. (2018) developed an extensive dataset of the morphological properties of drained depressions ( $n = 173,171$ ) in the DML-IA using hydrologically enforced digital elevation models (DEMs) of 3 m horizontal resolution derived from Light Ranging and Detection (LiDAR) data obtained for the Iowa Department of Natural Resources between 2007 and 2010. As discussed by these authors, unique relationships between incremental inundation depths, inundation areas, and storage volumes were derived for each topographically closed drained depression in the region using a custom geospatial algorithm implemented in the Python 2.7 programming language. McDeid and colleagues used these data to calculate the maximum inundation area ( $A_{max}$ ), maximum storage volume ( $V_{max}$ ), and maximum depth ( $H_{max}$ ) of each drained depressional feature in the region, and found that depressional morphologic characteristics vary across the DML-IA with, generally, deeper and smaller depressions in the north of the region, and shallower and larger depressions in the south.

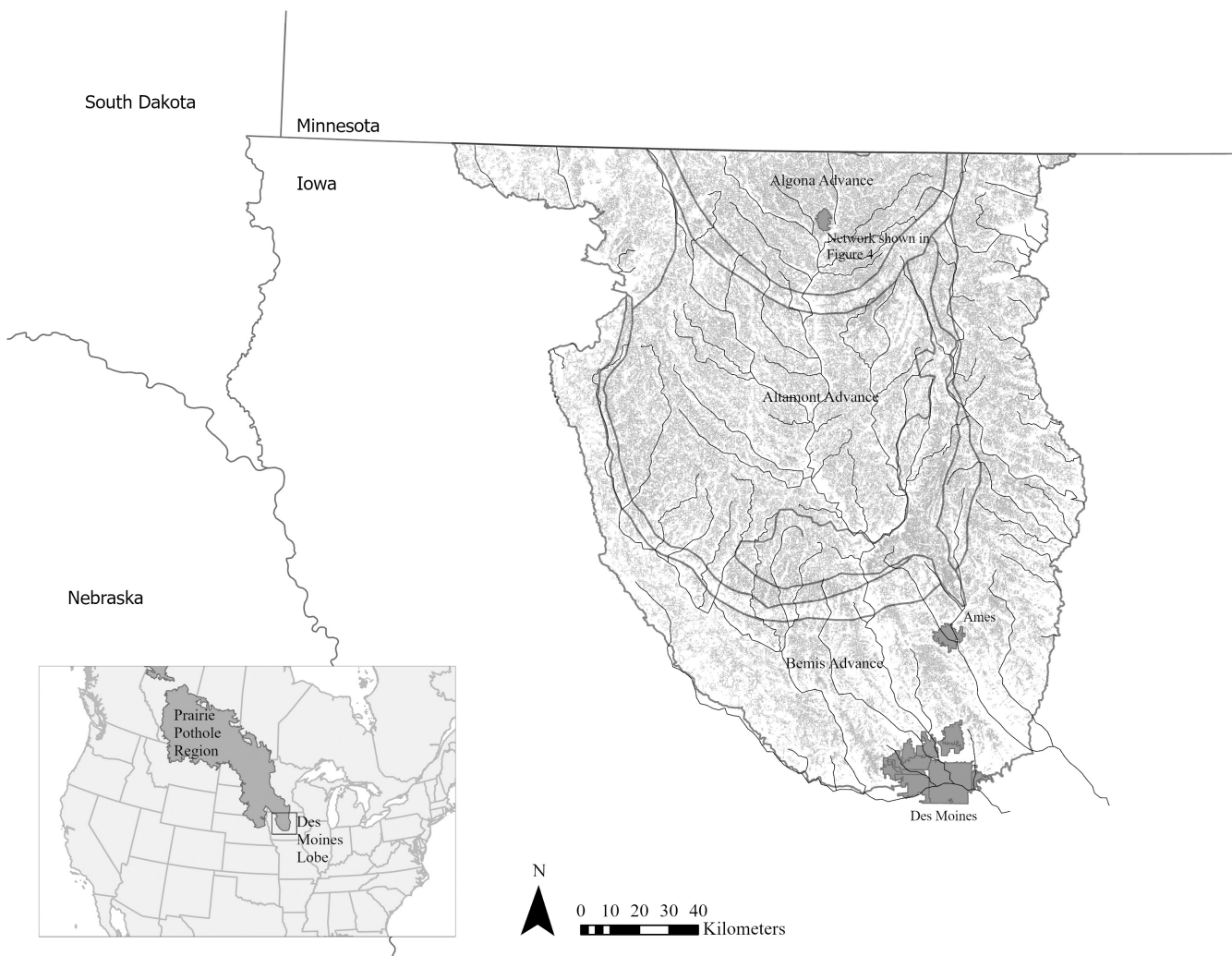


**FIGURE 5** DML-IA and the larger Prairie Pothole Region of North America. Small gray polygons within the boundary of the DML-IA represent the depressions delineated by McDeid et al. (2018). The east–west morainal bands represent the boundaries of the primary geomorphic sub-regions of the area. The major and minor stream networks illustrate the density of drainage within the region. Major cities in the region are given for reference. The depressional cascade network shown in Figure 4 is also given for reference. Adapted from Green et al. (2019).

The dataset developed by McDeid et al. (2018) was further refined for this study to remove non-depressional features that had been mistakenly included in prior work. Removed features primarily included previously overlooked depressions that overlap with existing homesteads and forested areas, as LiDAR return signals within areas of dense vegetation are more uncertain, and therefore, so are the estimates of depressional morphological attributes. The final dataset used in this work consisted of 167,287 depressional features, representing a 3.4% decrease in the number of features reported in McDeid et al. (2018). This refined set gives median and mean values of  $H_{\max}$ ,  $A_{\max}$ , and  $V_{\max}$  of 0.35 m, 0.47 ha, and 631 m<sup>3</sup>, and 0.43 m, 1.34 ha, and 5293 m<sup>3</sup>, respectively. Minimum and maximum values of these characteristics for the refined dataset used in this work are essentially unchanged from the values given in McDeid et al. (2018).

### 3.3 | DML-IA depressional cascade network development and analysis

The local catchments of each of the 167,287 depressions in the DML-IA were delineated using a D8 flow direction grid (Jenson & Domingue, 1988) derived from the same hydrologically enforced 3 m DEM used to estimate depressional morphology. The sets of upslope ( $m$ ) and downslope ( $k$ ) depressions for each depression were developed by iteratively finding geospatially adjoining upslope depression and downslope catchment features (which can be observed in Figure 1) and conducting iterative forward and backward searches on the dataset. The resulting database table of network connectivity, an example of which is given in Table 1, was used to classify each depression according to its landscape position, as defined earlier. All geospatial operations were performed using the Esri ArcGIS software platform.

**TABLE 2** Morphological attributes of depressions within the DML-IA organized by landscape position.  $A_{\max}$  is the maximum depression inundation area (ha),  $V_{\max}$  is the maximum depression storage volume ( $\text{Mm}^3$ ),  $A_{\text{cat}}$  is the local catchment area for each depression, and  $A_{\max}/A_{\text{cat}}$  is the ratio of depression maximum inundation area to local catchment area (—). Totals represent the sum of each attribute for each landscape position and for the region.

Landscape position	Number	Attribute	Median	Mean	Max	Min	Total
Disjunct	24,515	$A_{\max}$ (ha)	0.37	0.68	34.00	0.04	16,739
		$V_{\max}$ ( $\text{Mm}^3$ )	0.0005	0.002	0.56	<0.00001	44.19
		$A_{\text{cat}}$ (ha)	3.05	5.57	213.80	0.17	136,435
		$A_{\max}/A_{\text{cat}}$ (—)	0.14	0.16	0.82	0.0012	NA
Outlet	18,851	$A_{\max}$ (ha)	0.68	1.97	206.41	0.04	37,196
		$V_{\max}$ ( $\text{Mm}^3$ )	0.0089	0.0082	2.11	0.00001	153.28
		$A_{\text{cat}}$ (ha)	8.70	20.18	1217.06	0.17	380,384
		$A_{\max}/A_{\text{cat}}$ (—)	0.10	0.13	0.72	0.0003	NA
Mid-slope	53,464	$A_{\max}$ (ha)	0.74	2.26	193.71	0.04	120,854
		$V_{\max}$ ( $\text{Mm}^3$ )	0.0011	0.01	3.69	<0.00001	546
		$A_{\text{cat}}$ (ha)	6.77	14.69	850.87	0.16	785,560
		$A_{\max}/A_{\text{cat}}$ (—)	0.14	0.16	0.71	0.0002	NA
Headwater	70,457	$A_{\max}$ (ha)	0.36	0.69	42.72	0.04	48,795
		$V_{\max}$ ( $\text{Mm}^3$ )	0.0005	0.002	0.66	<0.00001	141.35
		$A_{\text{cat}}$ (ha)	2.55	4.46	294.11	0.06	314,243
		$A_{\max}/A_{\text{cat}}$ (—)	0.16	0.18	0.96	0.0019	NA
All (region)	167,287	$A_{\max}$ (ha)	0.47	1.34	206.41	0.04	223,584
		$V_{\max}$ ( $\text{Mm}^3$ )	0.0006	0.005	3.69	<0.00001	885.36
		$A_{\text{cat}}$ (ha)	3.91	9.66	1217.06	0.06	1,616,623
		$A_{\max}/A_{\text{cat}}$ (—)	0.15	0.17	0.96	0.0002	NA

Network connectivity between depressions was programmatically and manually evaluated to check for accuracy and directionality. This process resulted in identification of 24,515 disjunct, 70,457 headwater, 53,464 mid-slope, and 18,851 outlet depressions representing the outlets of each of the region's 18,851 distinct cascade networks (Table 2). All depression-specific morphological attributes, local catchment areas, and sets of upslope and downslope depressions were compiled into a database for subsequent application of the runoff routing algorithm and calculation of precipitation- and non-precipitation-dependent network properties.

Preliminary analyses showed that the distributions of each of the primary non-precipitation-dependent network properties exhibited heavy tailed behavior, with the exception of  $O_{st}$ . To identify the likely heavy tailed distributions representing these properties, we compared the log-likelihoods of fits to three probability distribution functions (PDFs) often observed in geophysical and hydrographic data: lognormal, power-law, and truncated power-law. Distribution fitting was performed by minimizing the Kolmogorov-Smirnov distance for each assessed PDF (Alstatt et al., 2014).

### 3.4 | DML-IA depressional cascade runoff routing

Two cases were examined in the routing of surface runoff through depressional cascade networks in the DML-IA: (1) uniform depths of precipitation applied over the entire region with no infiltration or other abstractions within the depressions or their local catchments and (2) uniform depths of precipitation of a range and interval identical to the previous case applied over the region with infiltration abstractions factored into estimates of precipitation excess, and therefore surface runoff. For each case, Equation (5) was recursively applied to each of the depressions in each of the 18,851 distinct depressional cascade networks, and each of the 24,515 disjunct depressions in the region. Following application of these equations, precipitation-dependent network properties as described in Equations (6) through (12) were calculated for all networks for all considered precipitation amounts, and aggregated and scaled to represent these quantities for the entire DML-IA. Both cases neglected evapotranspiration losses, the loss of water within depressions through surface water vertical intakes into underlying tile drains, and exfiltration of groundwater into depressions. In addition, both cases assumed that the entirety of each local depressional catchment contributed to surface runoff generation, and that there were no losses of water transported between depressions. For each precipitation amount, all depressions were assumed to be empty ( $V_0 = 0$ ) at the onset of rainfall, which is a likely normal condition for most drained depressions in this

landscape (McDeid et al., 2018). However, the assumption that depressions are empty at the onset of rainfall is not a necessary condition for employing the framework, and varied initial water storages will produce different depressional runoff routing and connectivity values, such as shown in Figure 4, for a given network and precipitation amounts.

### 3.4.1 | Case 1: Network routing without infiltration

For this case, infiltration abstractions within each local catchment and corresponding depression were neglected, and precipitation excess was assumed equal to the depth of rainfall,  $P$ . In application of the routing algorithms, precipitation amounts ranging from 1 to 320 mm, at intervals of 10 mm, were applied over the entirety of the set of depressional networks and each disjunct depression in the region. These precipitation amounts were selected to encompass the spatial average of the range of 1 through 500-year, 24-h rainfall events observed for the DML-IA (Perica et al., 2013). Treatment of the depressional networks as impervious surfaces permits evaluation of network routing processes absent the potentially confounding effects of infiltration on surface runoff generation, and provides upper limits on the degree of overland flow connectivity between depressions, network exports, and runoff contributing areas with varying precipitation amounts.

### 3.4.2 | Case 2: Network routing with infiltration

To assess depressional fill-spill patterns under more moderately realistic surface runoff conditions, we conducted the same analysis as for Case 1, but with precipitation excess determined using the U.S. Department of Agriculture (USDA) Natural Resources Conservation Service (NRCS) curve number runoff method (USDA NRCS, 1986).

Using the NRCS curve number methodology, precipitation excess was estimated for each depression and its local catchment from:

$$Q_{\text{cat}} + Q_{\text{prc}} = (A_{\text{cat}} + A_{\max}) \begin{cases} \frac{(P - 0.2S)^2}{P + 0.8S}; P > 0.2S \\ 0; 0 \leq P \leq 0.2S \end{cases}. \quad (19)$$

The quantity  $S$  (m) in Equation (19) represents the soil storage deficit required to be satisfied before ponding can occur in a given depression and surface runoff can occur within the local depressional catchment (Chow et al., 1988):

$$S = \frac{25.4}{\text{CNI}} - 0.254, \quad (20)$$

where CNI is the NRCS curve number for "dry" AMCI to account for the effects of tile drainage on reducing surface runoff in catchments with subsurface drainage networks. To estimate CNI values, area-weighted "normal" AMCI curve numbers (CNII) were determined for each depression and its catchment from available USDA NRCS SSURGO (U.S. Department of Agriculture Natural Resources Conservation Service, Soil Survey Geographic Database. Accessed June 2021, <https://sdmdataaccess.sc.egov.usda.gov>) hydrological soil group data for the region and the 2016 USGS NLCD dataset (U.S. Geological Survey National Land Cover Dataset. Accessed June 2021, <https://www.mrlc.gov/data>). CNII values were assigned to the geospatial intersection of each distinct hydrological soil group and land use classification according to the guidelines of Chow et al. (1988), with the assumption that all areas under row crop cultivation with subsurface tile drainage featured generally "good" hydrological conditions. Estimated CNII values were then adjusted downward to match AMCI conditions using (Chow et al., 1988):

$$\text{CNI} = \frac{4.2\text{CNII}}{10 - 0.058\text{CNII}}. \quad (21)$$

## 4 | RESULTS

### 4.1 | Depressional network characteristics

Depressional cascade networks and disjunct depressions and their local catchments comprise approximately 52.1% (1,616,623 ha) of the total drainage area of the DML-IA. Approximately 90% (1,454,961 ha) of this area is under row-crop cultivation, and approximately 80% of the soils of these networks are classified as poorly drained hydric-types, and thus are likely tile-drained (McDeid et al., 2018). Area-weighted NRCS AMCI curve numbers of depressional network catchments have a mean and median of 86 (characteristic of lands under row crop cultivation), and range from 49 in catchments characterized primarily by areas of densely vegetated pasturelands and deciduous woodlands, to 100 in

catchments primarily underlain by impervious surfaces, such as small network sub-catchments which overlap developed areas or which are comprised almost entirely of permanent or semi-permanent water bodies.

Across the region, local depressional contributing areas range from 0.06 to 1217.06 ha, with median and mean values of 3.91 and 9.66 ha, respectively. Likewise, maximum depressional inundation areas and storage volumes range from 0.04 to 206.41 ha and 6.57 m<sup>3</sup> to 3.69 Mm<sup>3</sup>, with median and mean values of 0.47 and 1.34 ha, and 631 and 5292 m<sup>3</sup>, respectively. Between landscape positions, outlet depressions tend to have the largest local contributing areas and maximum storage volumes, followed by mid-slope depressions (Table 2). Disjunct and headwater depressions tend to feature similarly sized local contributing areas, storage volumes, and maximum areas of inundation.

The 18,851 depressional cascade networks in the DML-IA range in number of depressions ( $n$ ) from 2 to 301, with median and mean counts of 3 and 8, respectively. Combined, depressions that are part of cascade networks of size  $n > 1$  (outlet, mid-slope, and headwater) constitute approximately 85.3% (142,772) of the total number of depressions in the region (Table 2), with disjunct depressions comprising the remainder (14.7%). The number of directly neighboring depressions ( $|m|$ ) within the region's cascade networks of size  $n > 1$  ranges from a minimum of 0 for headwater features to a maximum of 40 for mid-slope or outlet features, with a median of 1 and a mean of 2. In contrast, the number of downslope depressions ( $|k|$ ) ranges from a minimum of 0 for outlet features, to a maximum of 4, with a median and mean of 1 for mid-slope and headwater features.

Network Strahler order ( $O_{st}$ ) ranges from 1 to 4, with 48.4% of networks being of order 1, 47.6% being of order 2, and 4.0% being of order 3. Nine networks in the region are of order 4. Likewise, network Shreve order ( $O_{sh}$ ) ranges from 1 to 167, of which 48.4% are of order 1, 17.9% are of order 2, 8.7% are of order 3, and 5.3% are of order 4. The remaining 19.7% of networks are of higher Shreve orders, with 96 networks (0.51% of the total) having an order greater than or equal to 50.

Network branching order ( $O_b$ ) ranges from 0 to 72, and 48.4% of networks possess no branching depressions and are linear cascades of flow-connected features. These cascades correspond to first-order networks as defined either by the Shreve or Strahler algorithms. Approximately 26.2% of networks have one branching depression, 9.6% of networks have two, 4.8% of networks have three, and the remaining 11% of networks have more than three. Approximately 2.7% of networks are highly convoluted, possessing branching orders greater than 10.

Network area ( $A_{nw}$ ) ranges from 0.83 to 3417 ha, with median and mean values of 26.1 and 79.3 ha, respectively. Network depressional storage volume ( $V_{nw}$ ) ranges from 73.3 m<sup>3</sup> to 3.96 Mm<sup>3</sup>, with a median and mean values of 0.0063 and 0.045 Mm<sup>3</sup>, respectively. Likewise, network depressional specific storage ( $S_d$ ) ranges from 0.24 to 829 mm, with median and mean values of 26.8 and 42.6 mm, respectively. Network size,  $V_{nw}$ ,  $A_{nw}$ ,  $S_d$ , and all three measures of network complexity tend to be highest in the Algona Advance, and the eastern half of the Altamont Advance, and appear to be randomly distributed throughout the rest of the region (data not shown). These two regions are the youngest of the DML-IA's glaciated sub-regions, and possess higher densities of depressions, which also tend to have greater storage volumes and smaller local catchments (McDeid et al., 2018).

## 4.2 | Distributions of network properties

As shown in Figures 6 and 7 and listed in Table 3, over the range of available data,  $O_{sh}$  and  $O_b$  appear to conform to the truncated power-law distribution (Alstott et al., 2014). In contrast, network size  $n$ , the number of directly neighboring upslope depressions  $|m|$ , sub-network size (defined as the total number of potentially contributing depressions upslope of a feature,  $n_{sn}$ ),  $A_{nw}$ ,  $V_{nw}$ ,  $S_d$ , and network distance, defined as the number of downslope depressions between a given depression and the network outlet depression ( $n_d$ ; Shook et al., 2021), appear to conform to the lognormal distribution.

As shown in Figure 7, the distributions of network distance ( $n_d$ ), and this quantity normalized by network size, termed the fractional network distance ( $f_d$ ), suggest that most depressions in the region are clustered around network outlets, with nearly 84% of features belonging to groups comprising the 33.3% of depressions closest to their respective outlets. In contrast, very few depressions appear to be far removed from their network outlets, with less than 10% of features being within the farthest approximately 10% of depressions of their respective networks.

The fractional branching orders ( $f_b$ ) of networks in the region appear to be normally distributed, excluding networks with zero branches, with a median of 0.24, and a mean of approximately 0.25. This result indicates that, on average, 24% and 25% of the depressions in an average network are branched features. The mean and median of network fractional branching order,  $f_b$ , also appears to be close to a natural limit when plotted against  $O_{sh}$  (Figure 8), suggesting that as the complexity of networks increase, as implied by increasing values of  $O_{sh}$ , the likely number of branched features approaches approximately 24% of the total number of depressions. In addition, as also shown in Figure 8, our results suggest that network complexity (as defined by either  $O_{sh}$  or  $O_b$ ) appears to be reasonably described as a simple linear function of network size, indicating that larger networks tend also to be more complex in this region.

Considered in the aggregate, these findings indicate that the majority of depressional networks in the DML-IA are relatively small in size (50% of networks in the region contain fewer than 3 depressions), comprise relatively small areas on average, have comparatively little

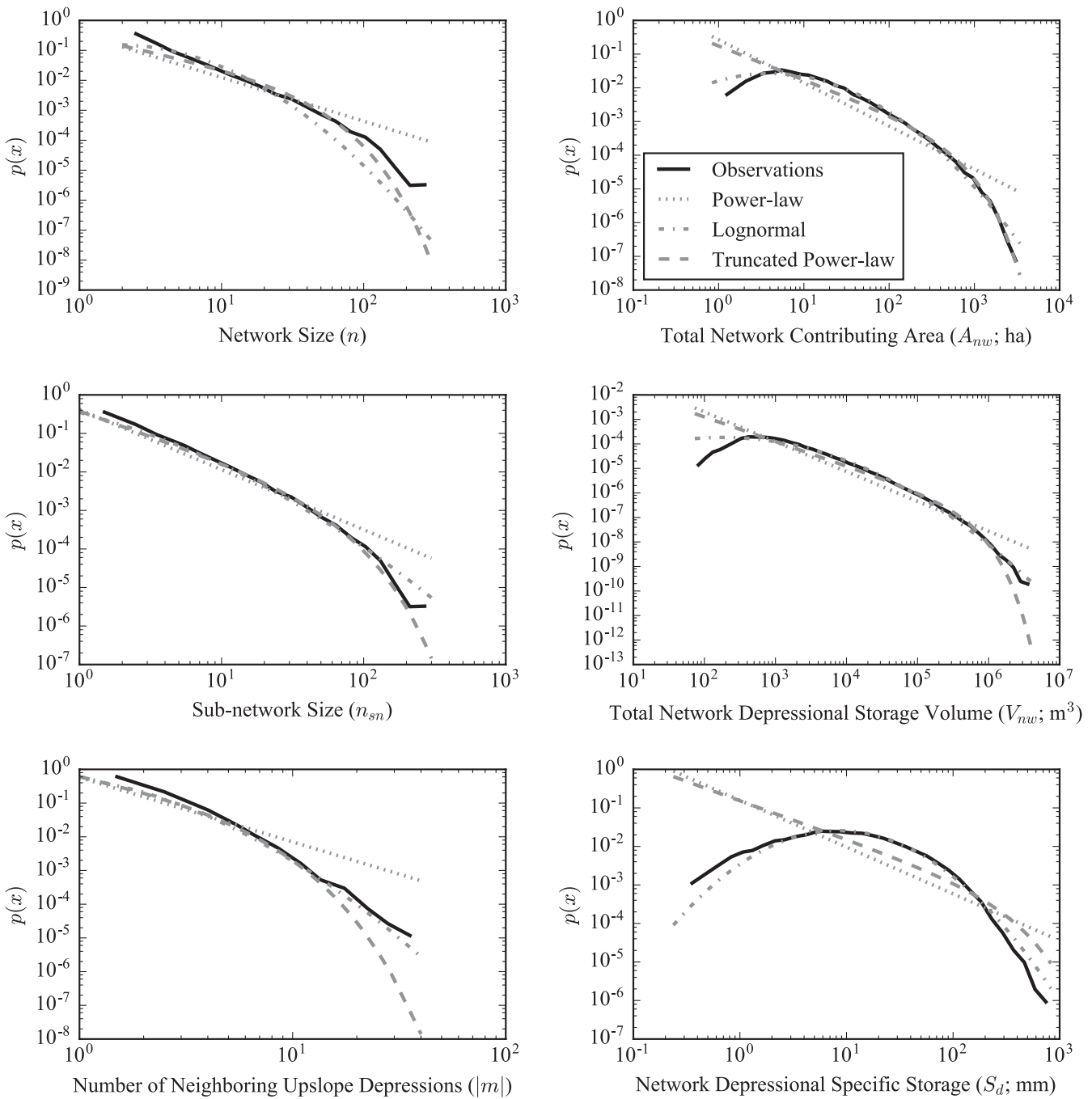


**FIGURE 6** Probability distributions and associated functions of network size ( $n$ ), sub-network size ( $n_{sn}$ ) defined as the size of the network upslope of each depression, the number of adjacent neighboring upslope depressions ( $|m|$ ), network contributing area ( $A_{nw}$ ; ha), network storage volume ( $V_{nw}$ ;  $\text{Mm}^3$ ), and network depressional specific storage ( $S_d$ ; mm) for the DML-IA.

aggregate storage capacity, and thus are able to retain only moderate amounts of surface runoff relative to likely quantities of precipitation, with the latter finding being consistent with the results of Green et al. (2019). Furthermore, our findings indicate that most of the networks contain depressions that are clustered around their respective network outlets, and have relatively simple branching and connectivity structures, based on the significant numbers of networks with low  $O_{sh}$ ,  $O_{st}$ , and  $O_b$  values (networks of order  $\leq 3$  for  $O_{sh}$  and  $O_{st}$  comprise 99.9% and 91.6% of networks, respectively). In addition, a significant number of networks are linear cascades comprised of unbranched chains of depressions. However, a few large networks exhibit highly complex branching structures and mid-slope or headwater clustering. Despite the preponderance of low-order networks, our results also suggest that small and intermediate sized networks ( $3 \leq n \leq 70$ ) might possess some self-similarity with respect to network structure, a characteristic that is also common to some stream channel systems (Mantilla et al., 2010; Yi et al., 2018).

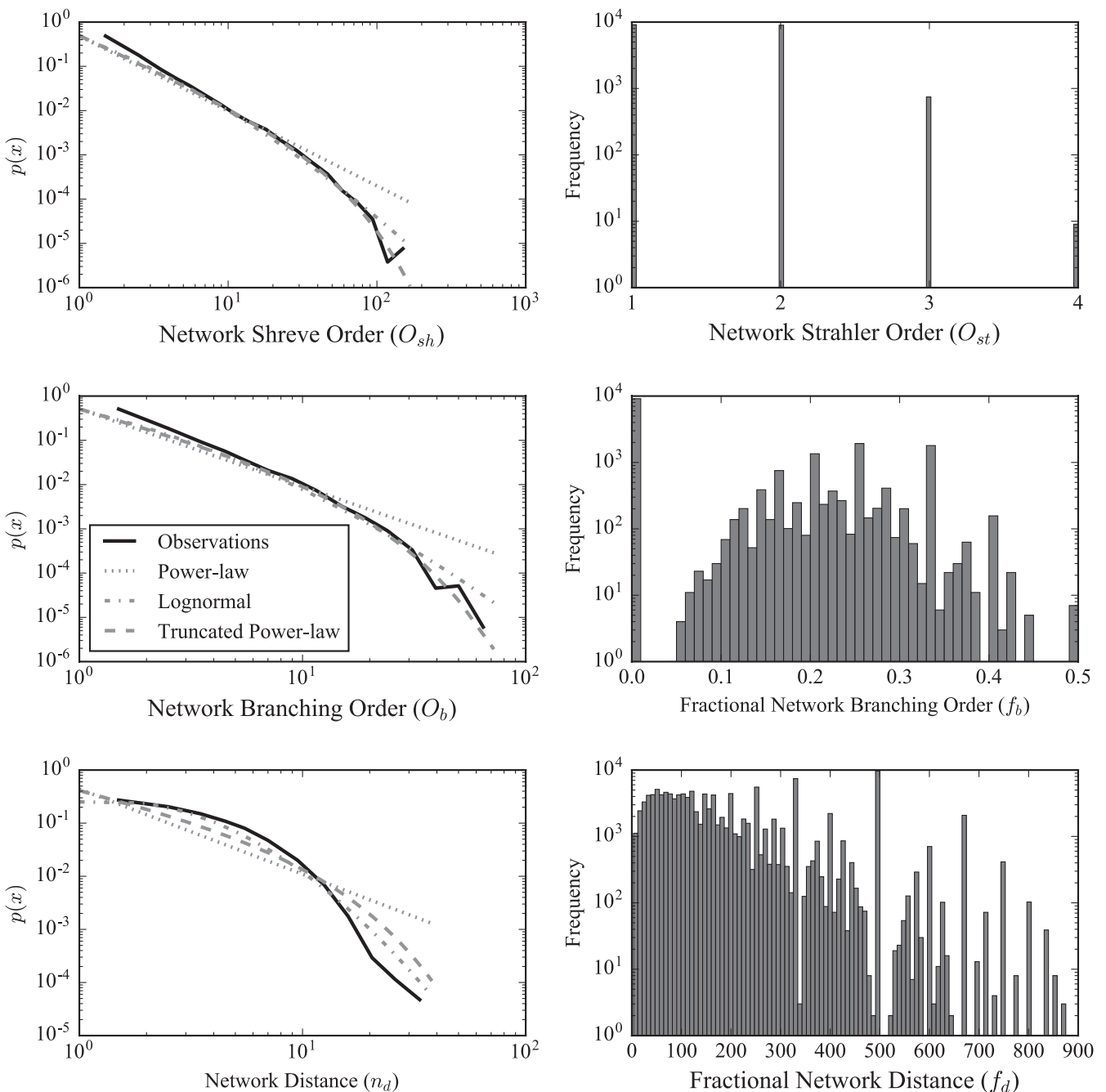


**FIGURE 7** Distributions of the measures of complexity for all depressional cascade networks of the DML-IA.  $O_{sh}$  is the network Shreve order.  $O_{st}$  is the network Strahler order.  $O_b$  and  $f_b$  are the network branching order and fractional branching order, respectively.  $n_d$  is the network distance, defined as the number of depressions between a feature and the network outlet depression.  $f_d$  is the network distance normalized by the size of the network ( $n$ ).

### 4.3 | Framework application results

For both cases, application of the framework for 33 distinct rainfall amounts applied to all depressions and corresponding networks in the DML-IA using the Python 2.7 programming language took 8.6 min to compute Case 1, and 6.8 min to compute Case 2, including computation of attendant precipitation-dependent network properties. These computation times correspond to averages of 15.7 and 12.3 s per rainfall amount, respectively.

**TABLE 3** Distribution fits and general statistics of some non-precipitation-dependent properties of depressional cascade networks of  $n > 1$  in the DML-IA. Discrete indicates that the fitting was performed on discrete integer values. Continuous indicates the fitting was performed on non-integer values. KS is the Kolmogorov-Smirnov distance of the fit. The truncated power-law distribution has one parameter:  $\alpha$ , the exponent. The lognormal distribution has two parameters:  $\mu$  and  $\sigma$ , the shape parameter and the standard deviation of the probability distribution function (PDF), respectively. PDF selection was based on a comparison of the log-likelihoods of tested distributions fit over the data range.

Network property	Min	Max	Mean	Median	Likely PDF	Fitted PDF parameters	KS
Network size ( $n$ )	2	301	3	8	Lognormal (discrete)	$\mu = 1.4488$ $\sigma = 0.9329$	0.1583
Sub-network size ( $n_{sn}$ )	1	300	2	7	Lognormal (discrete)	$\mu = 0.2279$ $\sigma = 1.6773$	0.0703
Number neighboring upslope depressions ( $ m $ )	0	40	1	2	Lognormal (discrete)	$\mu = -0.0828$ $\sigma = 0.9111$	0.0295
Network contributing area ( $A_{nw}$ ; ha)	0.83	3417	26.1	79.3	Lognormal (contin.)	$\mu = 12.5636$ $\sigma = 1.398$	0.0318
Network depressional storage volume ( $V_{nw}$ )	733 (m <sup>3</sup> )	3.96 (Mm <sup>3</sup> )	0.0063 (Mm <sup>3</sup> )	0.045 (Mm <sup>3</sup> )	Lognormal (contin.)	$\mu = 8.8769$ $\sigma = 1.9201$	0.0369
Network depressional specific storage ( $S_d$ ; mm)	0.24	829	26.8	42.6	Lognormal (contin.)	$\mu = 3.2428$ $\sigma = 1.0589$	0.0209
Network Shreve order ( $O_{sh}$ )	1	167	2	4	Truncated power-law (discrete)	$\alpha = 1.5498$	0.0877
Network branching order ( $O_b$ )	0	72	1	1	Truncated power-law (discrete)	$\alpha = 1.4016$	0.0719
Network distance ( $n_d$ )	1	38	3	4	Lognormal (discrete)	$\mu = 0.9085$ $\sigma = 0.8253$	0.05174
Network Strahler order ( $O_{st}$ )	1	4	2	2	—	—	—
Fractional branching order ( $f_b$ )	0	0.5	0.125	0.125	—	—	—
Fractional network distance ( $f_d$ )	<0.01	0.875	0.148	0.200	—	—	—

#### 4.3.1 | Case 1

As shown in Figures 9 and 10, under the assumptions of Case 1, the degree of surface runoff connectivity between depressions within all depressional cascade networks in the DML-IA, and therefore total network contributing areas, increases nonlinearly with increasing precipitation, as posited earlier. This is illustrated most clearly for the fraction of the total number of depressions contributing runoff to areas downslope of the networks ( $f_{ro}$ ) as a function of precipitation. In this case,  $f_{ro}$  is seen to increase rapidly with rainfall up to approximately 30 mm, which marks an inflection point beyond which the rate of increase in  $f_{ro}$  with increasing precipitation declines. At this precipitation amount, approximately 64.4% of depressions within the region have been filled to capacity and 45.5% are exporting excess runoff to downslope areas, with these features retaining 66.5% of total runoff ( $Q_{tot}$ ) comprising approximately 35% of total available depressional storage ( $V_{nw}$ ).

At the inflection point of  $f_{ro}$ , depressional networks that contribute runoff to areas downslope of local networks comprise approximately 51% of the total depressional network area of the region ( $f_{Aro}$ ), and 26.5% of the total area of the DML-IA. This part of the  $f_{ro}$  curve is dominated by the filling and spilling of outlet and next-in-sequence mid-slope features, particularly those with smaller storage volumes and larger local upslope network contributing areas. The inflection point represents a shift in flow contributions from primarily outlet depressions and depressions clustered near outlets, to primarily headwater and mid-slope depressions (Figure 11, top panel).

Precipitation amounts greater than 30 mm result in subsequent filling and spilling of successively larger depressions and greater numbers of headwater depressions, resulting in lower rates of increase of upslope contributing area, and of depressions contributing runoff from the networks. At the lower end of the range of precipitation for a 1-year, 24-h event, the fraction of depressions in the region that are contributing runoff to areas downslope of depressional networks is approximately 70%, which corresponds to an expansion of the total network contributing area within the region to approximately 70% (36.5% of the area of the DML-IA). At 320 mm, 99.2% of depressions in the region are contributing runoff to downslope areas, corresponding to 99% of total network contributing area (51.4% of the area of the DML-IA), and nearly 99.7% are filled, comprising approximately 96% of total available depressional storage, and storing and exporting approximately 17.7 and 82.3% of runoff, respectively.

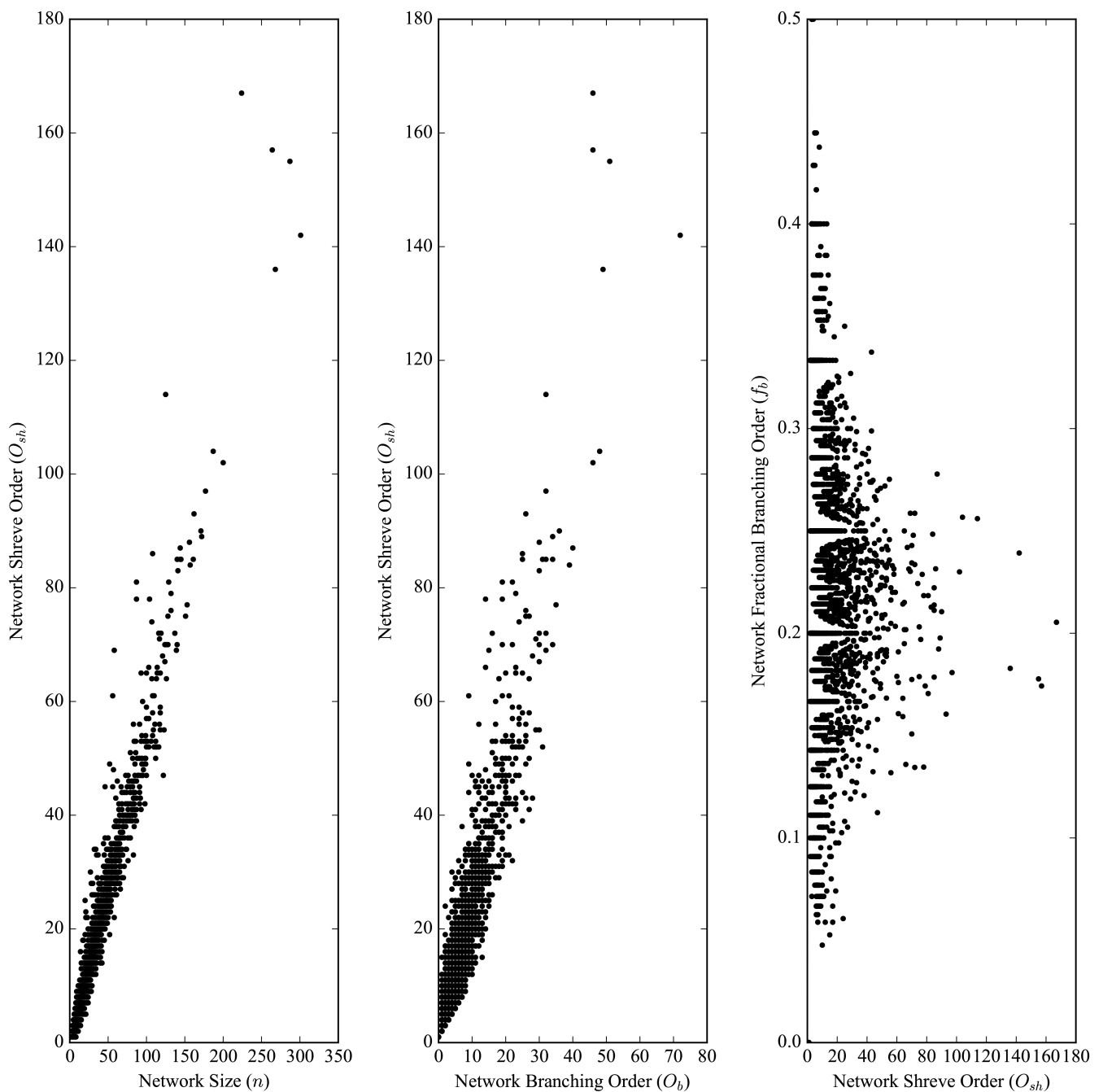


**FIGURE 8** Left panel: Network Shreve order ( $O_{sh}$ ) as a function of network size ( $n$ ). Middle panel: Network Shreve order ( $O_{sh}$ ) as a function of network branching order ( $O_b$ ). Right panel: Fraction network branching order ( $f_b$ ) as a function of  $O_{sh}$ .

#### 4.3.2 | Case 2

Under the assumptions of Case 2, which includes infiltration abstractions in estimates of surface runoff to and losses within depressions, export from the region's depressional networks does not begin to occur until approximately 20 mm of precipitation, and increases rapidly to approximately 70 mm, beyond which the rate of increase of the number of depressions contributing runoff, network contributing area, and filled network water storage begins to decline (Figure 12). At 60 mm of rainfall, roughly coinciding with the lower end of precipitation amounts expected for a 1-year, 24-h rain event, approximately 18.5% of depressions in the region contribute runoff from cascade networks, constituting approximately 30.3% of total network contributing area and 15.8% of the total drainage area of the DML-IA (Figures 12 and 13). At this precipitation amount, approximately 44.4% of depressions are filled to capacity, retaining approximately 76.8% of total runoff, with the remainder being exported to off-network areas. At the lower end of a 500-year, 24-h event, 96.2% of depressions are filled to their storage

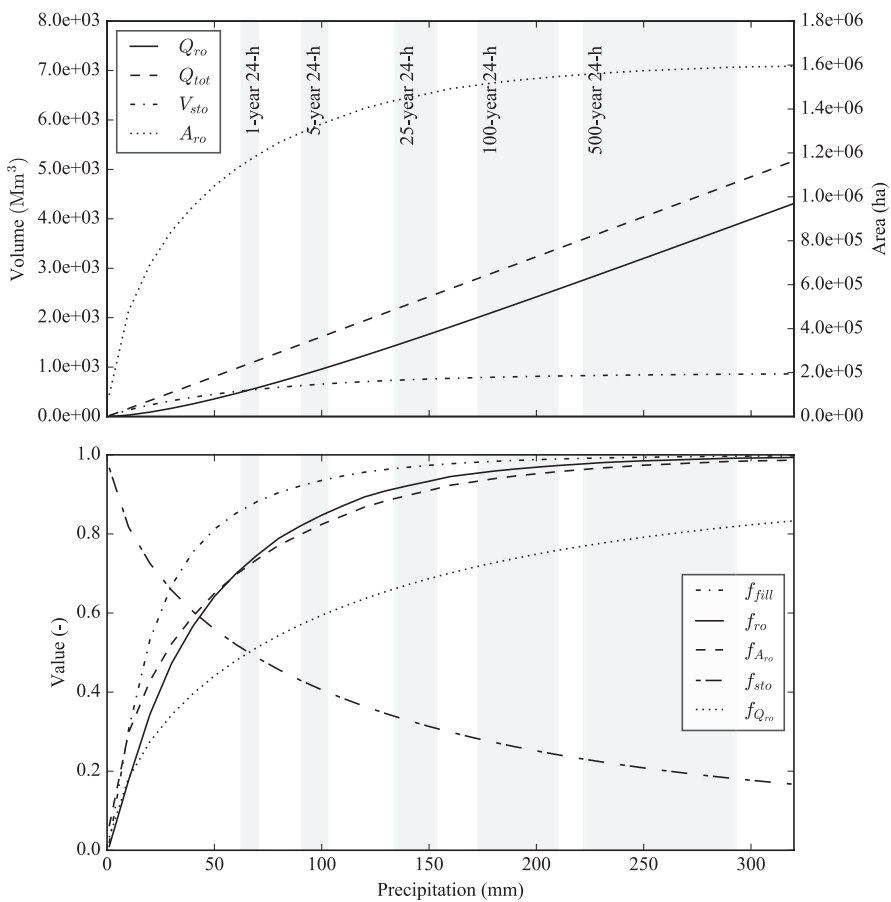


**FIGURE 9** Network properties as functions of precipitation amount aggregated for the entire DML-IA for Case 1 (neglecting abstractions in infiltration excess calculations). Top panel: Total network volumetric export ( $Q_{ro}$ ), volume of runoff stored ( $V_{sto}$ ), network runoff contributing area ( $A_{ro}$ ), and volume of runoff absent depressional storage ( $Q_{tot}$ ). Bottom panel: Fraction of depressions filled to capacity ( $f_{fill}$ ), fraction of depressions contributing runoff to network outlets and to areas downstream ( $f_{ro}$ ), the fraction of the total network area in the region contributing runoff to areas downstream of network outlets ( $f_{A_{ro}}$ ), the fraction of runoff stored in depressions ( $f_{sto}$ ), and the fraction of total runoff ( $Q_{tot}$ ) being exported from depressional networks ( $f_{Q_{ro}}$ ). The shaded gray regions represent the range of precipitation amounts seen within the DML-IA for 1, 5, 25, 100, and 500-year 24-h rain events.

capacities storing approximately 35% of runoff, with 90.9% of depressions in the region's networks contributing runoff to off-network areas, constituting 88.5% of total network contributing area in the DML-IA.

As with Case 1, the decline in the rate of increase in the considered precipitation-dependent properties marks the point at which exports from cascade networks shift from being dominated by outlet and mid-slope features, to being primarily driven by increasing connectivity of headwater and mid-slope features (Figure 11, bottom panel). The results from both cases suggest that runoff from these networks, and hydrological connectivity between depressions, expands upslope with increasing precipitation amounts, with outlet depressions having the greatest likelihood of being directly connected to off-network areas, a finding also supported by Evenson et al. (2018).

For both cases, the networks that export the least amount of surface runoff at lower precipitation amounts tend to be clustered in parts of the Algona and Bemis advances in the north central and east central sections of the DML-IA (Figures 10 and 13). Both areas are characterized by dense networks of depressions with significant aggregate water storage potential (Green et al., 2019; McDeid et al., 2018).

#### 4.3.3 | Effects of network structure on runoff connectivity patterns

Figures 14 and 15 show the mean fraction of depressions within the region contributing runoff to off-network areas ( $f_{ro}$ ) for Cases 1 and 2, organized by network size ( $n$ ),  $O_{st}$ , and for ranges of  $O_{sh}$  (and by extension  $O_b$ ) and  $S_d$ , representing observed natural breaks for the distributions of these network properties. In general, more complex networks, as defined by higher values of  $O_{sh}$  and  $O_{st}$ , appear to exhibit lower degrees of runoff connectivity than simpler networks, and more "gate-keeping" behavior. However, while network complexity clearly plays an important role in depressional runoff connectivity in this landscape, this effect is likely primarily a function of the tendency of network

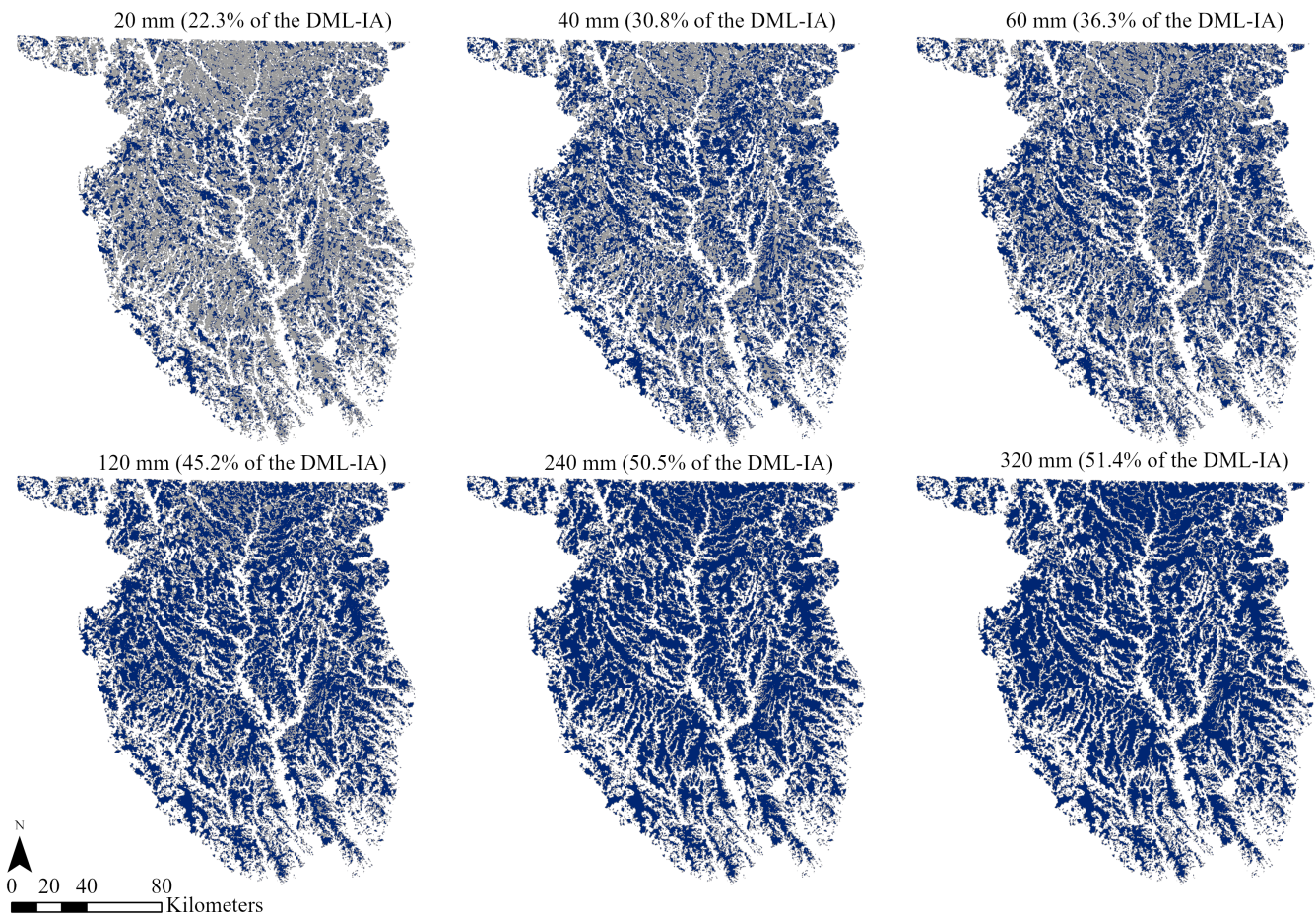


**FIGURE 10** Depressions within the DML-IA contributing runoff to off-network areas under various precipitation amounts applied uniformly over the region, neglecting infiltration or other abstractions (Case 1). Depressions that export runoff to off-network areas for a uniform depth of precipitation of 20mm under the assumptions of Case 1 comprise 22.3% of the total area of the region. This percentage increases rapidly with increasing precipitation depth.

complexity to increase with network size (left panel of Figure 8). This finding suggests that other factors such as the spatial distribution of depressional storage volumes and local contributing areas play a larger role in runoff connectivity between depressions in this landscape than network complexity as defined by the spatial arrangement of depressions within cascade networks. This is a conclusion also reached by Shook et al. (2021) in their analysis of the connectivity behavior of depressional networks in the St. Denis and Smith Creek research basins in Saskatchewan, Canada.

Indeed, as shown in panel 4 of Figures 14 and 15, networks with smaller total storage volumes and larger total contributing areas tend to exhibit greater degrees of connectivity at lower rainfall amounts (as defined by  $f_{ro}$ ), than do networks that feature larger cumulative storage volumes and smaller total contributing areas. For the former case (networks with smaller  $S_d$  values) runoff generated from smaller rainfall amounts tends to exceed both local depressional and cumulative network depressional storage capacities, resulting in relatively high degrees of runoff connectivity (as represented by the average fraction of runoff-connected depressions). For networks conforming to the latter case, as network  $S_d$  values increase greater amounts of rainfall are necessary to establish runoff connections between depressions, resulting in a concomitant increase in network gate-keeping behavior. Furthermore, the similarities between the two cases suggests that these patterns are relatively unaffected by the amount of runoff received by depressions within a network. There are no obvious patterns between average network distance and  $f_{ro}$  as functions of precipitation for either case (data not shown).

#### 4.4 | Validation of the framework and its application to the DML-IA for Case 2

Extensive validation of our routing algorithm for Case 2 to the entirety or even parts of the DML-IA is not feasible as the ponding dynamics within and runoff from and between depressions in this landscape is not routinely measured. However, a few studies have reported on the ponding dynamics of individual depressions in this region. For example, Schilling et al. (2019) measured groundwater elevations and ponded

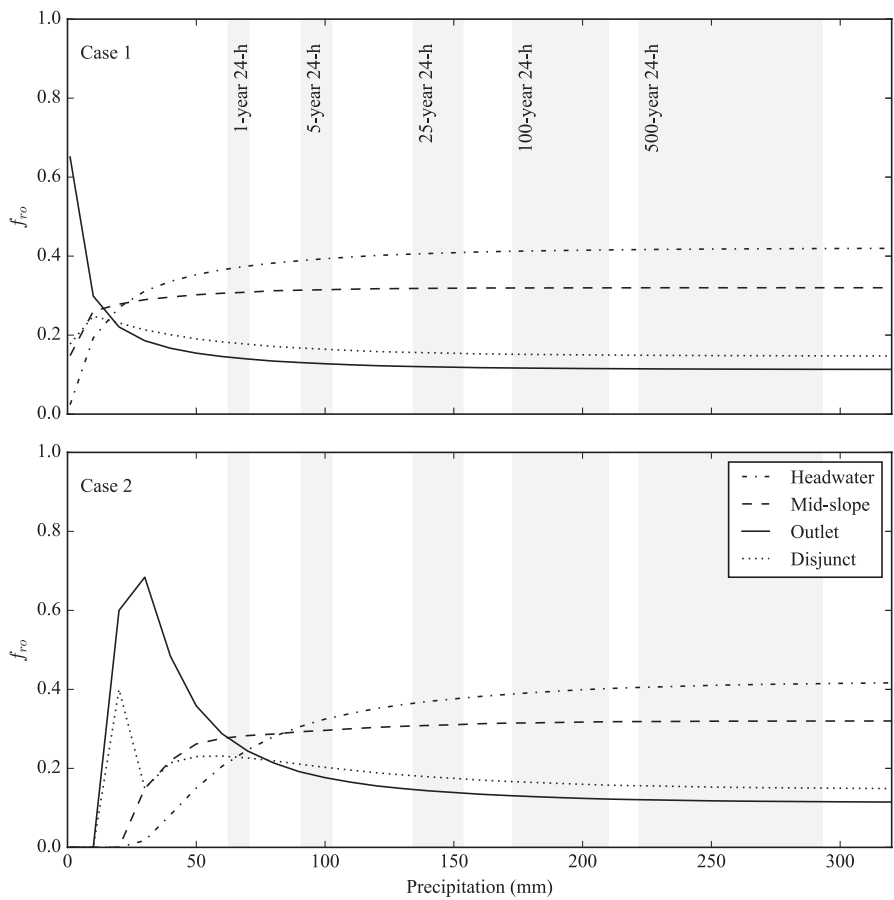


**FIGURE 11** The fractions of depressions contributing runoff to off-network areas ( $f_{r0}$ ) in the DML-IA for Cases 1 and 2, differentiated by depression type (landscape position). The shaded gray regions represent the range of precipitation amounts seen within the DML-IA for 1, 5, 25, 100, and 500-year 24-h rain events.

water levels in a 0.6 ha, 0.54 m deep drained headwater depression with a 3.4 ha local catchment in Hamilton County, Iowa for the period 2011 through 2013. During this time, the depression was not observed to spill, even after several moderately large ( $25 \leq P \leq 70$  mm) successive rain events in 2013. Our results from Case 2 suggest that this depression will fill and spill from rain events greater than 110 mm, an amount not exceeded during their study period.

Similarly, Martin et al. (2019) monitored the water levels of six depressions and sub-basin depressions within larger depressions with varying degrees of subsurface drainage in Story and Boone counties in central Iowa in 2016. Of the set of depressions, only one was observed to fill and spill. In this case, a headwater depression with no known subsurface drainage and possessing a local catchment area of 9.1 ha, a maximum storage volume of 1100 m<sup>3</sup>, and a maximum depth of 0.28 m exceeded its maximum storage capacity after a series of precipitation events that delivered 68 mm of rainfall over a 4-day period, resulting in 2287 m<sup>3</sup> of direct surface and shallow subsurface runoff into, and 580 m<sup>3</sup> of direct precipitation onto, the depression. Our results from Case 2 show that this depression has a fill-spill threshold of approximately 70 mm of precipitation, which is in close correspondence with the findings of Martin et al. (2019). However, the NRCS curve number method used in Case 2 estimates only approximately 1167 m<sup>3</sup> of direct runoff to this system for this threshold precipitation amount. For the remaining set of depressions, like Schilling et al. (2019), fill-spill behavior was not observed under the precipitation conditions encountered during the study; however, these depressions were each underlain by subsurface drains, and some had surface intakes (vertical drain pipes) serving as direct connections between the depressions and the underlying drainage tile. For Case 2, each of these depressions have precipitation-induced fill-spill thresholds of between 112 and 230 mm of rainfall; amounts not encountered during the Martin et al. (2019) study.

Finally, Roth and Capel (2012) observed fill-spill behavior in a 0.52 m deep, 1.3 ha drained sub-basin depression with approximately 3250 m<sup>3</sup> of potential storage volume within a larger encompassing outlet depression in Hamilton County, Iowa. The monitored depression, like some of the sites studied by Martin et al. (2019), featured directly underlying drainage tile and a surface water intake large enough to empty the depression from full within 48 to 68 h. Roth and Capel (2012) observed one fill and spill event in the sub-basin depression during the course of their study, caused by a storm that delivered approximately 40 mm of precipitation to the site, occurring after a series of rain events had left the depression and its catchment saturated, but not ponded. For Case 2, our framework shows that this sub-basin depression will fill and

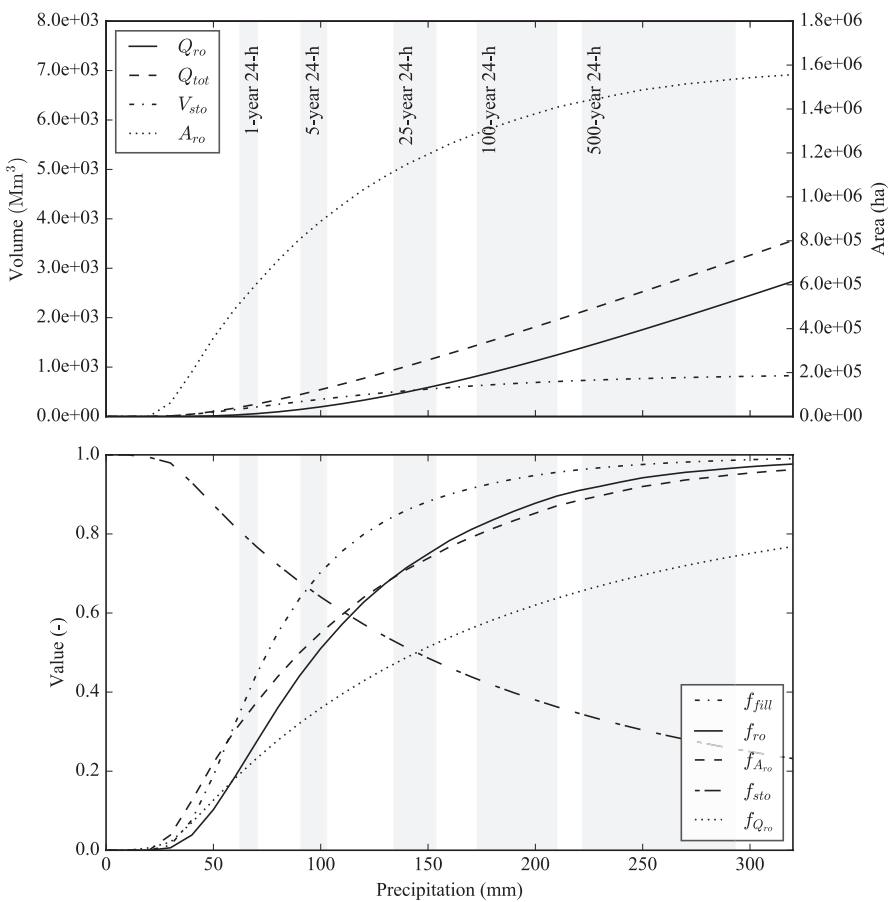


**FIGURE 12** Network properties as functions of precipitation, aggregated for the entire DML-IA for Case 2 (incorporating abstractions into precipitation excess calculations). Top panel: Total network volumetric export ( $Q_{ro}$ ), volume of runoff stored ( $V_{sto}$ ), contributing area ( $A_{ro}$ ), and runoff absent depressional storage ( $Q_{tot}$ ). Bottom panel: Fraction of depressions filled to capacity ( $f_{fill}$ ), fraction of depressions contributing runoff to network outlets and to off-network areas ( $f_{ro}$ ), the fraction of the total network area in the region contributing runoff to areas downstream of network outlets ( $f_{A_{ro}}$ ), the fraction of runoff stored in depressions ( $f_{sto}$ ), and the fraction of total runoff ( $Q_{tot}$ ) being exported from depressional networks ( $f_{Q_{ro}}$ ). The shaded gray regions represent the range of precipitation amounts seen within the DML-IA for 1, 5, 25, 100, and 500-year 24-h rain events.

spill from a storm event that delivers approximately 50 mm of precipitation, and will receive inflow from local runoff of  $3372 \text{ m}^3$  (results from Case 2 suggest that upslope depressions do not spill into this depression for this precipitation amount). These authors found that during this event, the monitored sub-basin received approximately  $6460 \text{ m}^3$  of runoff, comprised of, but not differentiated between, shallow groundwater exfiltration and direct overland flow from the depressional catchment.

The discrepancies between the magnitudes of the influxes of water into the depressions monitored by Roth and Capel (2012) and Martin et al. (2019) and amounts estimated from Case 2 is likely due to inaccuracies in precipitation excess amounts estimated by the NRCS curve number method in these catchments (Garen & Moore, 2005), as well as a lack of accounting for groundwater exfiltration in Case 2. In addition, for Roth and Capel (2012), the presence of vertical intakes was not accounted for in Case 2, which in this case likely enhanced available storage of the depression. Thus, in the absence of a vertical intake, it is likely that this sub-basin depression would require significantly less water to fill and spill than what was reported by Roth and Capel (2012).

Although threshold rainfall amounts were not observed during the Schilling et al. (2019) study, and were observed for only one depression out of six in the Martin et al. (2019) study, we consider the lack of observations of fill and spill behavior for these depressions, also predicted from Case 2, to at the very least not be a refutation of the general reasonableness of our framework. However, two reasonable (Martin et al., 2019; Roth & Capel, 2012) and seven potential points of agreement (Martin et al., 2019; Schilling et al., 2019) are not sufficient to verify the veracity of the framework or its application in Case 2, and additional confirmation is needed to further assess its accuracy. This will require either the use of remote sensing data with high spatial and temporal resolution (for example Brooks et al., 2018; Vanderhoof et al., 2016), direct in field monitoring of ponding and hydrological fluxes (Leibowitz & Vining, 2003; Martin et al., 2019; Roth & Capel, 2012), or, preferably, a combination of these approaches, efforts which are only beginning in the in DML-IA.

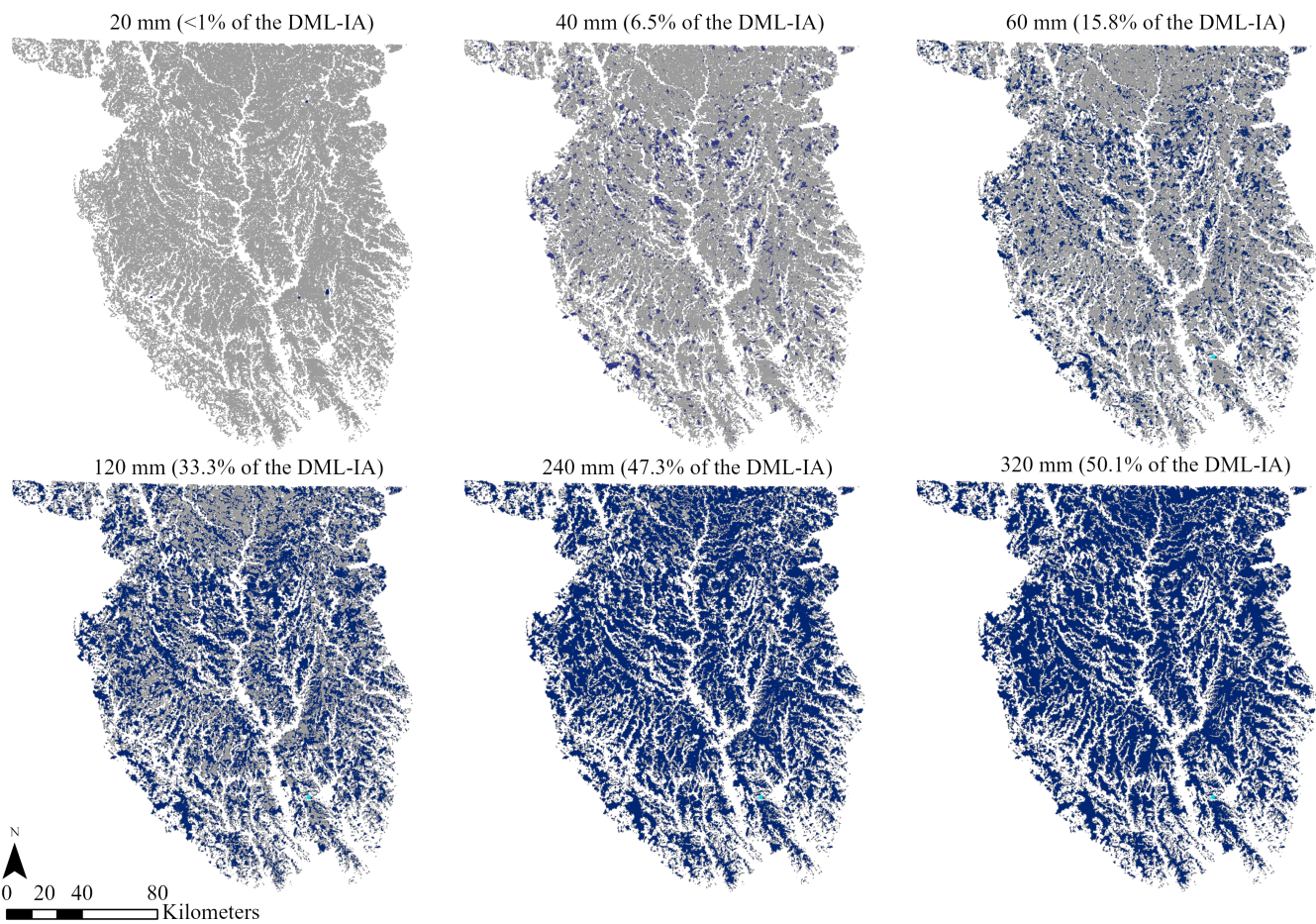


**FIGURE 13** Depressions within the DML-IA contributing runoff to off-network areas under various precipitation amounts applied uniformly over the region with abstractions factored into estimates of precipitation excess (Case 2). Depressions that export runoff excess for a uniform depth of precipitation of 40 mm under the assumptions of Case 2 comprise 6.5% of the total area of the region. This percentage moderately increases with increasing precipitation depth relative to Case 1. This effect is likely due to abstractions implicit with the Natural Resources Conservation Service curve number method reducing precipitation excess estimates, and not to the characteristics of the region's depressional cascade networks.

## 5 | DISCUSSION

### 5.1 | Assumptions and limitations

Our proposed framework is a simplified representation of the time-integrated routing of overland flow between surface depressions in a network, and cannot be used to simulate and evaluate time-dependent hydrological processes, such as assessing the effects that depressions have on flood hydrograph magnitude and duration, or quantifying the instantaneous fluxes of water into and out of these systems. However, as demonstrated in this study, this framework, based on fundamental hydrological principles, can be used to derive the structural properties of depressional cascade networks both small and large, including measures of network complexity, and evaluate the likelihood of surface flow connectivity of depressions under a range of precipitation amounts and surface runoff generation conditions using reasonable estimates of water budget fluxes. Furthermore, while significant simplifications of the hydrology of depressional landscapes were employed in this work, notably our assumption that the entirety of each local depressional catchment contributes precipitation excess to the receiving depression, our framework is flexible enough to be extended to include additional flows including groundwater connectivity or enhanced infiltration into tile or other drainage systems, and to include variable source areas (Dahlke et al., 2009; McDonnell, 2013) within depressional catchments.

Application of the framework is not restricted to specific models of infiltration or other losses and gains of water within cascade networks. For example, the NRCS curve number method was used in Case 2 primarily because of its simplicity and the ability to reasonably estimate spatially varying infiltration abstractions and precipitation excess amounts. Precipitation excess (and by definition infiltration and evapotranspiration abstractions) could have instead been estimated using any reasonable model of cumulative infiltration whether or not as a function of AMC and precipitation intensity and duration, or from extrapolation of direct infiltration measurements at smaller scales.

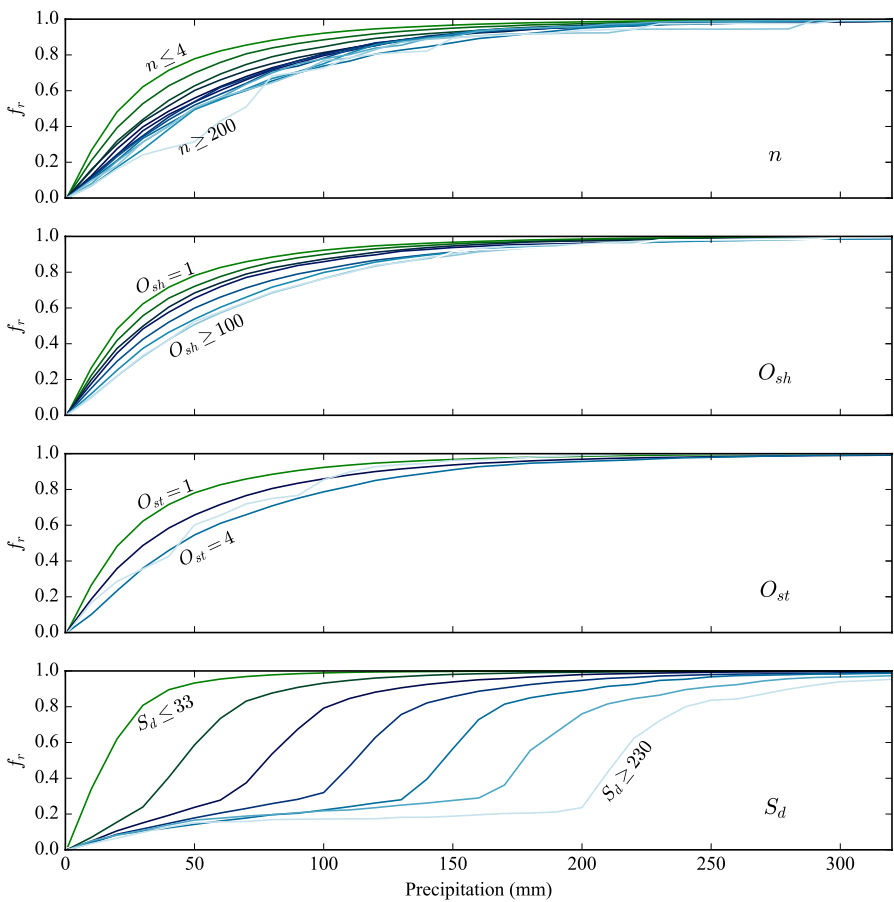


**FIGURE 14** Mean fraction of depressions within the cascade networks of the DML-IA contributing runoff to off-network areas as a function of precipitation amount under the assumptions of Case 1 aggregated by network size (top panel), network Shreve order ( $O_{sh}$ ) (second panel), network Strahler order ( $O_{st}$ ) (third panel), and network specific storage ( $S_d$ , m) values (fourth panel). Each line represents an average of  $f_{ro}$  for each precipitation amount for values or ranges of each network characteristic. In general, as network size, complexity, or the storage volume to contributing area ratio increases, the mean fraction of depressions across all networks within the DML-IA contributing runoff to off-network areas for a given precipitation amount decreases. However, of these factors,  $S_d$  is observed to have the largest influence on runoff connectivity between depressions and between depressional networks and off-network areas.

Similarly, groundwater exfiltration can be included using reasonable assumptions about local and regional water table elevations and appropriate models of groundwater responses to infiltration of surface water (see, e.g., Schilling et al., 2019). In addition, the water balance presented in Equation (2) does not distinguish between exfiltration of local groundwater and exfiltration of shallow subsurface through-flow between depressions. While this simplification is not necessarily restrictive for the DML-IA, where fill-spill processes are driven by precipitation excess overland flow and direct rainfall and exfiltrated groundwater is generally a small portion of the water budgets of these systems except for very wet periods (Roth & Capel, 2012; Schilling et al., 2018), it may not be a reasonable restriction in other areas (see, e.g., Hayashi et al., 2016; LaBaugh et al., 2018; McLaughlin et al., 2014).

There are several additional shortcomings to the work presented here, the first of which is the current restriction of single precipitation events being the primary forcing in application of the framework. This restriction is implemented for simplicity, and is not strictly necessary since integration of dynamic storage volumes of a depression and the fluxes of water which dictate its magnitude and variability can be integrated over arbitrary time periods and for varying magnitudes of rainfall and precipitation excess, even when individual fluxes, and thus water budget components, have zero magnitude. In addition, although both runoff routing cases explored in this work assumed spatially uniform precipitation amounts, this assumption is also not a requirement for application of the runoff routing algorithm. Indeed, it is feasible to apply the framework to a landscape using spatially varying precipitation amounts, such as from regional precipitation frequency estimates (Green et al., 2019; Perica et al., 2013).

Finally, this work shows two contrasting applications of the proposed framework: neglecting rainfall abstractions (Case 1), and incorporating spatially variable surface runoff accounting for rainfall abstractions (Case 2). As discussed previously, the first case was employed to remove the potentially confounding effects of water losses on the retention and transference of surface runoff between depressions, and permit a direct assessment of the relative effects of network complexity, and depression and catchment characteristics, on hydrological connectivity

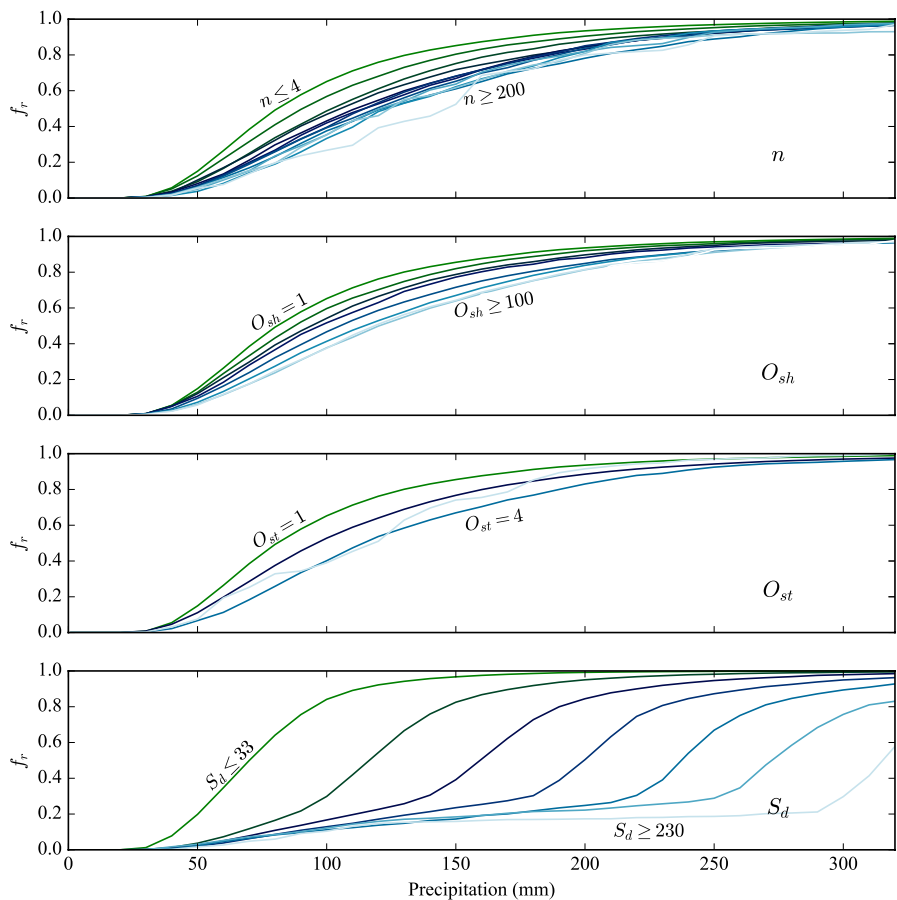


**FIGURE 15** Mean fraction of depressions within the cascade networks of the DML-IA contributing runoff to off-network areas as a function of precipitation amount under the assumptions of Case 2 aggregated by network size (top panel), network Shreve order ( $O_{sh}$ ) (second panel), network Strahler order ( $O_{st}$ ) (third panel), and network specific storage ( $S_d$ , m) values (fourth panel). Each line represents an average of  $f_{ro}$  for each precipitation amount for values or ranges of each network characteristic. As with Figure 14, of these factors,  $S_d$  is observed to have the largest influence on hydrologic connectivity between depressions and between depressional networks and off-network areas.

in this landscape. As such, Case 1 represents an upper limit to the collective effect of precipitation on surface runoff retention and transferance between depressions, in a manner similar to the analysis of Green et al. (2019). Case 2, in contrast, was intended to demonstrate the application of the framework to the DML-IA under more realistic assumptions about runoff generation in this landscape. In this case, considering the potentially significant uncertainty of the NRCS curve number estimates of runoff (Durán-Barroso et al., 2017) in the DML-IA, the results given in Case 2 are considered to be preliminary estimates of possible network cascade behavior, despite reasonable agreement between this and other works, as discussed previously. Indeed, and the points of agreement with the work of Martin et al. (2019) and Roth and Capel (2012) notwithstanding, it is possible that the results from Case 2 over-estimate connectivity between depressions under most of the precipitation amounts considered. For example, depending on rainfall and soil moisture conditions, a significant amount of runoff from upslope depressions may be lost to infiltration and evapotranspiration while in transit to receiving depressions, potentially resulting in significant surface run-on between depressions (Corradini et al., 1998; Figure 2), thereby reducing their overland flow connectivity.

## 5.2 | Comparison with other network-based approaches to depressional cascades

While there are numerous examples of model-based approaches to depressional fill-spill hydrology (e.g., Evenson et al., 2018; Haan & Johnson, 1968; Shaw et al., 2012, 2013; Shook et al., 2021; among others), there are very few network-based hydro-geomorphological approaches to this topic. The studies in closest correspondence to our approach to analyzing depressional fill-spill cascades are the works of Shook et al. (2021), Shaw et al. (2013), and Phillips et al. (2011). In these studies, these researchers demonstrated that connectivity between flow systems—lakes connected by streams in the case of Phillips et al. (2011), and depressional wetlands connected by overland flow pathways in the cases of Shook et al. (2021) and Shaw et al. (2013)—increases with increasing flows, but that the degree of this connectivity is primarily

influenced by basin and catchment morphological and land cover characteristics, and network structure and complexity to a lesser degree. Our findings are in accordance with the observations of these authors. For instance, Figures 9 through 15 show in various ways that as precipitation increases in the DML-IA more depressions contribute runoff to downslope areas resulting in greater degrees of hydrological connectivity between depressional networks and receiving off-network flow systems (this is also intuitively expected). In addition, as Figures 14 and 15 show, for a given amount of precipitation it is primarily the geomorphological structure of depressions and their local catchments (such as their contributing areas and available storage volumes and the combination of these characteristics) that ultimately dictates whether a portion of a network will be hydrologically connected to downslope features. Combined, these findings suggest that there are strong commonalities between seemingly disparate and geographically separate threshold-controlled surface flow systems, at least with respect to lakes, ponds, and depressions. Indeed, our results and those of Shook et al. (2021), Shaw et al. (2013), and Phillips et al. (2011) appear to at least moderately support the conceptual framework proposed by Buttle (2006) who suggested that runoff responses of individual drainage basins can be described by the relative influences of typology (partitioning between lateral and vertical hydrological storages), topography (landforms, including relative slopes), and topology (network properties, including measures of complexity). However, significantly more research is necessary to draw definitive conclusions about the relative effects of depressional cascade network complexity and morphology on hydrological connectivity in the PPR and elsewhere.

In this work, we also present alternate algorithms of the Strahler (1952, 1957) and Shreve (1966) stream order numbering schemes ( $O_{st}$  and  $O_{sh}$ , respectively) modified to be applied to depressional cascade networks. These adjusted numbering schemes, along with our proposed network branching order and fractional branching order metrics ( $O_b$  and  $f_b$ ), provide a relatively straightforward and standardized approach to assigning numerical values to depressional network complexity. While our representation of these numbering schemes are a modification of established approaches, our estimates are reasonably close to those of other researchers, at least with respect to Strahler numbers. For example, our Strahler numbers are similar in range to estimates given by Callaghan and Wickert (2019) for depressional networks within the Sangamon River watershed in Illinois and the Rio Toro watershed in Argentina, and to values reported by Shook et al. (2021) for depressional cascades in research catchments in Saskatchewan, Canada, both of whom presented values between 1 and 6. In both studies, Strahler orders were calculated using standard flow line network generation algorithms whereby the orders of depressions are determined by imposing flow line orders calculated from DEM-derived overland flow paths onto the depressional landscape. This approach is potentially complicated and effected by the spatial resolution of the DEM and the flow accumulation threshold used to derive the flow network (Helmlinger et al., 1993; Wang & Yin, 1998). In contrast, our algorithms orient the Strahler and Shreve numbering schemes to depressions, and rely on these features alone. Thus, we argue that our approach to calculating numerical values of depressional network complexity through the proposed modified Strahler and Shreve order algorithms is more appropriate for these types of systems. Furthermore, we demonstrate that using the landscape position classification scheme presented in this work (and an accounting of flow-connected directly neighboring depressions) the modified Shreve order of a network can be reasonably estimated from the number of depressions that have more than one directly neighboring upslope depression ( $|m| > 1$ ), further reducing the computational complexity of the approach presented here. To our knowledge, Shreve orders, branching orders, and fractional branching orders of depressional cascade networks have not been presented elsewhere in the literature.

### 5.3 | Potential applications of the framework

The simplicity and scalability of our framework makes it suitable for use in several areas, including increasing our understanding of the effects of networks of threshold-controlled systems on runoff across spatial scales, improving dynamic rainfall-runoff models in depressional landscapes and other similar systems, investigating the roles of depressional cascades on flood abatement, and providing valuable information for depressional wetland and upland ecosystem conservation and restoration efforts. For example, our framework could be applied, in a manner similar to its application to the DML-IA, to other regions of the PPR with a significant number of drained depressions, such as in southwestern Minnesota (Kessler & Gupta, 2015), or with similar effect to more intact depressional landscapes. Such work could provide critical information to landscape ecologists, hydrologists, and natural resources managers in this and similar regions that might aid in wetland ecosystem restoration and protection efforts, such as identifying wetlands or wetland complexes for targeted restorations that have a high likelihood of having flow connections under certain rainfall amounts. In this same vein, researchers could use outputs from application of the framework to select wetlands for further field studies of depressional fill and spill processes and their effects on water quality and local flood abatement. The framework could also be used on other landscapes outside of the PPR that feature significant numbers of depressional wetlands (Jones et al., 2018; Kirkman et al., 2012; McLaughlin et al., 2014).

In addition, this framework could be employed in parallel with a companion distributed or semi-distributed rainfall-runoff model of hydrologic processes in depressional landscapes as a check on model predictions for fill and spill processes, or to expand predictive power. For instance, Haan and Johnson (1968) developed and tested a semi-distributed model of coupled depression-mediated surface and subsurface flows to evaluate the effects of depressions on hydrograph attenuation, as well as the effects of subsurface drainage on depressional hydrology. In their model, these researchers aggregated depressions into lumped storages at the bases of local catchments. Our framework could

be used to expand on this and other similar models to provide a greater degree of realism. In addition, our framework could be expanded to incorporate time-varying processes (work that is currently in development), which could allow for simulation of the dynamic filling and spilling of depressions at spatial scales similar to the work presented here.

Finally, this framework can be one of a suite of approaches for evaluating the potential for hydrological connectivity among depressions as well as other threshold-controlled flow systems (Tromp-van Meerveld & McDonnell, 2006 for example) at multiple scales in the context of determining connected waters of the U.S., protected under the Clean Water Act (Alexander, 2015; Leibowitz et al., 2018). Employed within a probabilistic framework for selecting precipitation and runoff likelihoods, our algorithms could be used with suitable estimates of likely infiltration abstractions and other depressional water balance fluxes to evaluate the likelihood and potential magnitude of hydrological connections between depressions and between depressional cascade networks and downstream systems. This, in turn, may help scientists, land managers, and regulators to clarify further what constitutes hydrologically connected landscapes.

## 6 | SUMMARY AND CONCLUSIONS

In this study, we present a formal computational framework for efficiently routing ephemeral surface runoff through depressional runoff cascade networks of arbitrary size and complexity within a geographic region given information about depression morphology, existing water storage, and overland flow connectivity, and for characterizing the properties of these networks, precipitation-dependent or otherwise. The framework was applied to the entirety of the set of 167,287 delineated drained wetland depressions within the DML-IA, in part to demonstrate its usefulness for analyzing potential overland flow connections within large fill-spill cascade networks, as well as to derive information pertaining to network structure and potential surface runoff connectivity of depressions within this landscape.

Application of the framework to the DML-IA reveals that 85.3% of drained depressions in this region of the PPR form 18,851 unique depressional cascade networks, with the remainder being disjunct, non-networked, features. Network size ranges from 2 to 301 depressions; however, most networks within the region are primarily comprised of a small number of depressions, with median and mean sizes of 3 and 8 features, respectively. Networks range in total area from 0.83 to 3417 ha, and total depressional storage volume from 73.3 m<sup>3</sup> to 3.96 Mm<sup>3</sup>. In total, depressional cascade networks comprise 52.1% of the total drainage area of the DML-IA. The majority of these networks have relatively simple branching structures, with approximately 74.6% of networks featuring one or fewer branching depressions, corresponding to network Strahler and Shreve orders of ≤2. However, a few networks feature highly complex branching structures, with the remaining 25.4% of networks featuring Shreve orders of up to 167, Strahler orders of up to 4, and up to 72 branching depressions.

Fitting of possible heavy-tailed probability distributions to measured depressional cascade network properties suggests that network Shreve and branching orders likely follow a truncated power-law distribution. Network characteristics such as network size, sub-network size, network distance, network contributing area, network depressional storage volume, network depressional specific storage, and the number of directly neighboring upslope depressions each likely follow a lognormal distribution. In addition, our results suggest that network branching order is a reasonable predictor of network Shreve order, and that network complexity tends to increase with network size.

The results of routing precipitation excess through each depressional cascade network within the DML-IA suggest that the spatial distributions of depressional storage volumes and contributing areas within networks, and not network complexity, are the primary determinants of potential inter-depressional flow connectivity; findings that are in accordance with other studies. This, in turn, determines whether a given cascade network contributes surface runoff to off-network areas such as local swales and streams.

We believe that this framework is an important step in the process of implementing a formal, standard methodology for deriving the flow connectivity characteristics and general properties of depressional cascade networks at the landscape scale, and for conducting analyses of runoff routing between flow systems across spatial scales. Our algorithms could be applied to a variety of threshold-controlled fill-spill flow systems to develop additional information about the structure of cascade networks, and assess the likelihood of their surface runoff connectivity under a range of hydrological conditions. Such analyses may produce valuable information in support of, for example, sub-regional and regional hydrological model development efforts, flood abatement studies, and wetland conservation and restoration planning.

## AUTHOR CONTRIBUTIONS

**David I. S. Green:** Conceptualization; data curation; formal analysis; funding acquisition; investigation; methodology; project administration; resources; software; validation; visualization; writing – original draft; writing – review and editing. **William G. Crumpton:** Conceptualization; resources; writing – review and editing.

## ACKNOWLEDGMENTS

The authors thank Dr. Greg Stenback and several anonymous reviewers for their valuable input. Open access funding provided by the Iowa State University Library.

## CONFLICT OF INTEREST STATEMENT

Neither author has conflicts of interest to disclose that pertain to this work.

## DATA AVAILABILITY STATEMENT

The Python 2.7 code developed for this project is available from the corresponding author upon request, or can be accessed at <https://github.com/disgreen/DepressionalNetworkCascade>.

## ORCID

David I. S. Green  <https://orcid.org/0000-0002-9343-3926>

## REFERENCES

- Alexander, L.C. 2015. "Science at the Boundaries: Scientific Support for the Clean Water Rule." *Freshwater Science* 24(4): 1588–94.
- Alstott, J., E. Bullmore, and D. Plenz. 2014. "powerlaw: A Python Package for Analysis of Heavy-Tailed Distributions." *PLoS One* 9(1): e85777. <https://doi.org/10.1371/journal.pone.0085777>.
- Barnes, R., K.L. Callaghan, and A.D. Wickert. 2020. "Computing Water Flow through Complex Landscapes—Part 2: Finding Hierarchies in Depressions and Morphological Segmentations." *Earth Surface Dynamics* 8: 431–45. <https://doi.org/10.5194/esurf-8-431-2020>.
- Barnes, R., K.L. Callaghan, and A.D. Wickert. 2021. "Computing Water Flow through Complex Landscapes—Part 3: Fill–Spill–Merge: Flow Routing in Depression Hierarchies." *Earth Surface Dynamics* 9: 105–21. <https://doi.org/10.5194/esurf-9-105-2021>.
- Bishop, R.A., A.J. Joens, and J. Zohrer. 1998. "Iowa's Wetlands, Present and Future with a Focus on Prairie Potholes." *Journal of the Iowa Academy of Science* 88: 11–16.
- Bracken, L.J., and J. Croke. 2007. "The Concept of Hydrological Connectivity and Its Contribution to Understanding Runoff-Dominated Geomorphic Systems." *Hydrological Processes* 21: 1749–63. <https://doi.org/10.1002/hyp.6313>.
- Brooks, J.R., D.M. Mushet, M.K. Vanderhoof, S.G. Leibowitz, J.R. Christensen, B.P. Neff, D.O. Rosenberry, W.D. Rugh, and L.C. Alexander. 2018. "Estimating Wetland Connectivity to Streams in the Prairie Pothole Region: An Isotopic and Remote Sensing Approach." *Water Resources Research* 54(2): 955–77. <https://doi.org/10.1002/2017WR021016>.
- Buttle, J. 2006. "Mapping First-Order Controls on Streamflow from Drainage Basins: The T3 Template." *Hydrological Processes* 20(15): 3415–22. <https://doi.org/10.1002/hyp.6519>.
- Callaghan, K.L., and A.D. Wickert. 2019. "Computing Water Flow through Complex Landscapes—Part 1: Incorporating Depressions in Flow Routing Using Flowfill." *Earth Surface Dynamics* 7(3): 737–53. <https://doi.org/10.5194/esurf-7-737-2019>.
- Chow, V.T., D.R. Maidment, and L.W. Mays. 1988. *Applied Hydrology*. New York: McGraw-Hill.
- Chu, X., J. Yang, Y. Chi, and J. Zhang. 2013. "Dynamic Puddle Delineation and Modeling of Puddle-to-Puddle Filling-Spilling-Merging-Splitting Overland Flow Processes." *Water Resources Research* 49: 3825–29. <https://doi.org/10.1002/wrcr.20286>.
- Cohen, M.J., I.F. Creed, L. Alexander, N.B. Basu, A.J.K. Calhoun, C. Craft, E. D'Amico, et al. 2016. "Do Geographically Isolated Wetlands Influence Landscape Functions?" *Proceedings of the National Academy of Sciences of the United States of America* 113(8): 1978–86.
- Corradini, C., R. Morbidelli, and F. Melone. 1998. "On the Interaction between Infiltration and Hortonian Runoff." *Journal of Hydrology* 204(1–4): 52–67.
- Dahlke, H.E., Z.M. Easton, D.R. Fuka, S.W. Lyon, and T.S. Steenhuis. 2009. "Modelling Variable Source Area Dynamics in a CEAP Watershed." *Ecohydrology* 2(3): 337–49.
- Driscoll, J.M., L.E. Hay, M. Vanderhoof, and R.J. Viger. 2020. "Spatiotemporal Variability of Modeled Watershed Scale Surface-Depression Storage and Runoff for the Conterminous United States." *Journal of the American Water Resources Association* 56(1): 16–29. <https://doi.org/10.1111/1752-1688.12826>.
- Durán-Barroso, P., J. González, and J.B. Valdés. 2017. "Sources of Uncertainty in the NRCS CN Model: Recognition and Solutions." *Hydrological Processes* 31(22): 3898–906.
- Evenson, G.R., H.E. Golden, C.R. Lane, D.L. McLaughlin, and E. D'Amico. 2018. "Depressional Wetlands Affect Watershed Hydrological, Biogeochemical, and Ecological Functions." *Ecological Applications* 28(4): 953–66. <https://doi.org/10.1002/eap.1701>.
- Garen, D.C., and D.S. Moore. 2005. "Curve Number Hydrology in Water Quality Modeling: Uses, Abuses, and Future Directions." *Journal of the American Water Resources Association* 41(2): 377–88.
- Green, D.I.S., S.M. McDeid, and W.G. Crumpton. 2019. "Runoff Storage Potential of Drained Upland Depressions on the Des Moines Lobe of Iowa." *Journal of the American Water Resources Association* 55(3): 543–58. <https://doi.org/10.1111/1752-1688.12738>.
- Grimm, K., and X. Chu. 2018. "Modeling of Spatiotemporal Variations in Runoff Contribution Areas and Analysis of Hydrologic Connectivity." *Land Degradation and Development* 29(8): 2629–443. <https://doi.org/10.1002/lrd.3076>.
- Haan, C.T., and H.P. Johnson. 1968. "Hydraulic Model of Runoff from Depressional Areas Part 1: General Considerations." *Transactions of the American Society of Agricultural Engineers* 11(3): 368–73. <https://doi.org/10.13031/2013.39412>.
- Haque, A., G. Ali, and P. Badiou. 2018. "Hydrological Dynamics of Prairie Pothole Wetlands: Dominant Processes and Landscape Controls under Contrasted Conditions." *Hydrological Processes* 32: 2405–22. <https://doi.org/10.1002/hyp.13173>.
- Hayashi, M., G. van der Kamp, and D.O. Rosenberry. 2016. "Hydrology of Prairie Wetlands: Understanding the Integrated Surface-Water and Groundwater Processes." *Wetlands* 36: 237–54. <https://doi.org/10.1007/s13157-016-0797-9>.
- Helmlinger, K.R., P. Kumar, and E. Foufoula-Georgiou. 1993. "On the Use of Digital Elevation Model Data for Hortonian and Fractal Analyses of Channel Networks." *Water Resources Research* 29(8): 2599–613. <https://doi.org/10.1029/93WR00545>.
- Huang, S.L., C. Young, O.I. Abdul-Aziz, D. Dahal, M. Feng, and S.G. Liu. 2013. "Simulating the Water Budget of a Prairie Potholes Complex from LiDAR and Hydrological Models in North Dakota, USA." *Hydrological Sciences Journal* 58(7): 1434–44.
- Jenson, S.K., and J.O. Domingue. 1988. "Extracting Topographic Structure from Digital Elevation Data for Geographic Information System Analysis." *Photogrammetric Engineering and Remote Sensing* 54(11): 1593–600.

- Jones, C.N., G.R. Evenson, D.L. McLaughlin, M.K. Vanderhoof, M.W. Lang, G.W. McCarty, H.E. Golden, C.R. Lane, and L.C. Alexander. 2018. "Estimating Restorable Wetland Water Storage at Landscape Scales." *Hydrological Processes* 32(2): 305–13. <https://doi.org/10.1002/hyp.11405>.
- Kessler, A.C., and S.C. Gupta. 2015. "Drainage Impacts on Surficial Water Retention Capacity of a Prairie Pothole Watershed." *Journal of the American Water Resources Association* 51(4): 1101–13. <https://doi.org/10.1111/jawr.12288>.
- Kirkman, L.K., L.L. Smith, and S.W. Golladay. 2012. "Southeastern Depressional Wetlands." In *Wetland Habitats of North America: Ecology and Conservation Concerns*, edited by Darold P. Batzer and Andrew H. Baldwin, 203–16. Oakland, CA: University of California Press.
- LaBaugh, J.W., D.O. Rosenberry, D.M. Mushet, B.P. Neff, R.D. Nelson, and N.H. Euliss, Jr. 2018. "Long-Term Changes in Pond Permanence, Size, and Salinity in Prairie Pothole Region Wetlands: The Role of Groundwater-Pond Interaction." *Journal of Hydrology: Regional Studies* 17: 1–23.
- LaBaugh, J.W., T.C. Winter, and D.O. Rosenberry. 1998. "Hydrologic Functions of Prairie Wetlands." *Great Plains Research* 8: 17–37.
- Lanfear, K.J. 1990. "A Fast Algorithm for Automatically Computing Strahler Stream Order." *Journal of the American Water Resources Association* 26(6): 977–81.
- Leibowitz, S.G., D.M. Mushet, and W.E. Newton. 2016. "Intermittent Surface Water Connectivity: Fill and Spill vs. Fill and Merge Dynamics." *Wetlands* 36(Suppl 2): 323–42. <https://doi.org/10.1007/s13157-016-0830-z>.
- Leibowitz, S.G., and K.C. Vining. 2003. "Temporal Connectivity in a Prairie Pothole Complex." *Wetlands* 23: 13–25. [https://doi.org/10.1672/0277-5212\(2003\)023\[0013:TCIAPP\]2.0.CO;2](https://doi.org/10.1672/0277-5212(2003)023[0013:TCIAPP]2.0.CO;2).
- Leibowitz, S.G., P.J. Wigington, K.A. Schofield, L.C. Alexander, M.K. Vanderhoof, and H.E. Golden. 2018. "Connectivity of Streams and Wetlands to Downstream Waters: An Integrated Systems Framework." *Journal of the American Water Resources Association* 54(2): 298–322. <https://doi.org/10.1111/1752-1688.12631>.
- Mantilla, R., B.M. Troutman, and V.K. Gupta. 2010. "Testing Statistical Self-Similarity in the Topology of River Networks." *Journal of Geophysical Research* 115. <https://doi.org/10.1029/2009JF001609>.
- Martin, A., A.L. Kaleita, and M.L. Soupir. 2019. "Inundation Patterns of Farmed Pothole Depressions with Varying Subsurface Drainage." *Transactions of the American Society of Agricultural and Biological Engineers* 62(6): 1579–90.
- Marton, J.M., I.F. Creed, D.B. Lewis, C.R. Lane, N.B. Basu, M.J. Cohen, and C.B. Craft. 2015. "Geographically Isolated Wetlands Are Important Biogeochemical Reactors on the Landscape." *Bioscience* 65(4): 408–18. <https://doi.org/10.1093/biosci/biv009>.
- McDeid, S.M., D.I.S. Green, and W.G. Crumpton. 2018. "Morphology of Drained Upland Depressions on the Des Moines Lobe of Iowa." *Wetlands* 39: 587–600.
- McDonnell, J.J. 2013. "Are all Runoff Processes the Same?" *Hydrological Processes* 27: 4103–11. <https://doi.org/10.1002/hyp.10076>.
- McDonnell, J.J., C. Spence, D.J. Karra, H.J. van Meerveld, and C.J. Harman. 2021. "Fill-And-Spill: A Process Description of Runoff Generation at the Scale of the Beholder." *Water Resources Research* 57(5): e2020WR027514. <https://doi.org/10.1029/2020WR027514>.
- McLaughlin, D.L., J.S. Diamond, C. Quintero, J. Heffernan, and M.J. Cohen. 2019. "Wetland Connectivity Thresholds and Flow Dynamics from Stage Measurements." *Water Resources Research* 55: 6018–32. <https://doi.org/10.1029/2018WR024652>.
- McLaughlin, D.L., D.A. Kaplan, and M.J. Cohen. 2014. "A Significant Nexus: Geographically Isolated Wetlands Influence Landscape Hydrology." *Water Resources Research* 50(9): 7153–66.
- Miller, B.A., W.G. Crumpton, and A.G. van der Valk. 2009. "Spatial Distribution of Historical Wetland Classes on the Des Moines Lobe, Iowa." *Wetlands* 29: 1146–52. <https://doi.org/10.1672/08-158.1>.
- Miller, B.A., W.G. Crumpton, and A.G. van der Valk. 2012. "Wetland Hydrologic Class Change from Prior to European Settlement to Present on the Des Moines Lobe, Iowa." *Wetlands Ecology and Management* 20: 1–8. <https://doi.org/10.1007/s11273-011-9237-z>.
- Neri, A., G. Villarini, L.J. Slater, and F. Napolitano. 2019. "On the Statistical Attribution of Flood Event across the U.S. Midwest." *Advances in Water Resources* 127: 225–36. <https://doi.org/10.1016/j.advwatres.2019.03.019>.
- Perica, S., D. Martin, S. Pavlovic, I. Roy, M. St Laurent, C. A. R. L. Trypaluk, D. Unruh, M. Yekta, and G. Bonnin. 2013. "NOAA Atlas 14 Volume 8 Version 2, Precipitation-Frequency Atlas of the United States, Midwestern States." NOAA National Weather Service Report.
- Phillips, R.W., C. Spence, and J.W. Pomeroy. 2011. "Connectivity and Runoff Dynamics in Heterogeneous Basins." *Hydrological Processes* 25: 3061–75. <https://doi.org/10.1002/hyp.8123>.
- Prior, J.C. 1991. *Landforms of Iowa*. Iowa City: University of Iowa Press.
- Rains, M., S.G. Leibowitz, M.J. Cohen, I.F. Creed, H.E. Golden, J.W. Jawitz, P. Kalla, C.R. Lane, M.W. Lang, and D.L. McLaughlin. 2016. "Geographically Isolated Wetlands Are Part of the Hydrological Landscape." *Hydrological Processes* 30: 153–60.
- Rothe, J.L., and P.D. Capel. 2012. "The Hydrology of a Drained Topographical Depression within an Agricultural Field in North-Central Iowa." *Transactions of the American Society of Agricultural and Biological Engineers* 55(5): 1801–14. <https://doi.org/10.13031/2013.42367>.
- Schilling, K.E., P.J. Jacobson, M.T. Streeter, and C.S. Jones. 2018. "Groundwater Hydrology and Quality in Drained Wetlands of the Des Moines Lobe in Iowa." *Wetlands* 38: 247–59.
- Schilling, K.E., S.R. Then, and C.D. Ikenberry. 2019. "Water Balance Modeling of Temporary Ponding in a Drained Prairie Pothole Wetland." *Environmental Modeling & Assessment* 24: 37–48. <https://doi.org/10.1007/s10666-018-9596-4>.
- Shaw, D.A., A. Pietroniro, and L. Martz. 2013. "Topographic Analysis for the Prairie Pothole Region of Western Canada." *Hydrological Processes* 27: 3105–14. <https://doi.org/10.1002/hyp.9409>.
- Shaw, D.A., G. Vanderkamp, F.M. Conly, A. Pietroniro, and L. Martz. 2012. "The Fill-Spill Hydrology of Prairie Wetland Complexes during Drought and Deluge." *Hydrological Processes* 26: 3147–56. <https://doi.org/10.1002/hyp.8390>.
- Shook, K., S. Papalexiou, and J.W. Pomeroy. 2021. "Quantifying the Effects of Prairie Depressional Storage Complexes on Drainage Basin Connectivity." *Journal of Hydrology* 593: 125846. <https://doi.org/10.1016/j.jhydrol.2020.125846>.
- Shook, K.R., and J.W. Pomeroy. 2011. "Memory Effects of Depressional Storage in Northern Prairie Hydrology." *Hydrological Processes* 25: 3890–98. <https://doi.org/10.1002/hyp.8381>.
- Shreve, R.L. 1966. "Statistical Law of Stream Numbers." *Journal of Geology* 74(1): 17–37.
- Spence, C. 2007. "On the Relation between Dynamic Storage and Runoff: A Discussion on Thresholds, Efficiency, and Function." *Water Resources Research* 43: W12416. <https://doi.org/10.1029/2006WR005645>.
- Spence, C. 2010. "A Paradigm Shift in Hydrology: Storage Thresholds across Scales Influence Catchment Runoff Generation." *Geography Compass* 4: 819–33. <https://doi.org/10.1111/j.1749-8198.2010.00341.x>.

- Stichling, W., and S.R. Blackwell. 1957. "Drainage Area as a Hydrologic Factor on the Glaciated Canadian Prairies." Prairie Farm Rehabilitation Administration, Hydrology Division Report 365-376, Regina, Saskatoon, Canada.
- Strahler, A.N. 1952. "Hypsometric (Area-Altitude) Analysis of Erosional Topography." *GSA Bulletin* 63(11): 1117-42. [https://doi.org/10.1130/0016-7606\(1952\)63\[1117:HAAOET\]2.0.CO;2](https://doi.org/10.1130/0016-7606(1952)63[1117:HAAOET]2.0.CO;2).
- Strahler, A.N. 1957. "Quantitative Analysis of Watershed Geomorphology." *Transactions of the American Geophysical Union* 38(6): 913-20.
- Tromp-van Meerveld, H.J., and J.J. McDonnell. 2006. "Threshold Relations in Subsurface Stormflow: 2. The Fill and Spill Hypothesis." *Water Resources Research* 42: W02411. <https://doi.org/10.1029/2004WR003800>.
- USDA NRCS. 1986. "Urban Hydrology for Small Watersheds" Technical Release Report 55 (TR-55). Washington: Natural Resources Conservation Services, USDA.
- van der Valk, A. 2005. "Prairie Potholes of North America." In *The World's Largest Wetlands*, edited by Lauchlan Fraser and Paul Keddy, 393-423. Cambridge, UK: Cambridge University Press.
- Vanderhoof, M.K., L.C. Alexander, and M.J. Todd. 2016. "Temporal and Spatial Patterns of Wetland Extent Influence Variability of Surface Water Connectivity in the Prairie Pothole Region, United States." *Landscape Ecology* 31: 805-24. <https://doi.org/10.1007/s10980-015-0290-5>.
- Wang, X., and Z.-Y. Yin. 1998. "A Comparison of Drainage Networks Derived from Digital Elevation Models at Two Scales." *Journal of Hydrology* 210(1-4): 221-41. [https://doi.org/10.1016/S0022-1694\(98\)00189-9](https://doi.org/10.1016/S0022-1694(98)00189-9).
- Wu, Q., and C.R. Lane. 2017. "Delineating wetland catchments and modeling hydrologic connectivity using lidar data and aerial imagery." *Hydrology and Earth System Sciences* 21(7): 3579-3595. <https://doi.org/10.5194/hess-21-3579-2017>.
- Yi, R.S., A. Arredondo, E. Stansifer, H. Seybold, and D.H. Rothman. 2018. "Shapes of River Networks." *Proceedings of the Royal Society A* 474: 20180081. <https://doi.org/10.1098/rspa.2018.0081>.

**How to cite this article:** Green, D.I.S., and W.G. Crumpton. 2023. "Depressional runoff cascade networks of the Des Moines Lobe of Iowa." *JAWRA Journal of the American Water Resources Association* 00 (0): 1-31. <https://doi.org/10.1111/1752-1688.13103>.